Abstracta

Ano XXVII - N. 05

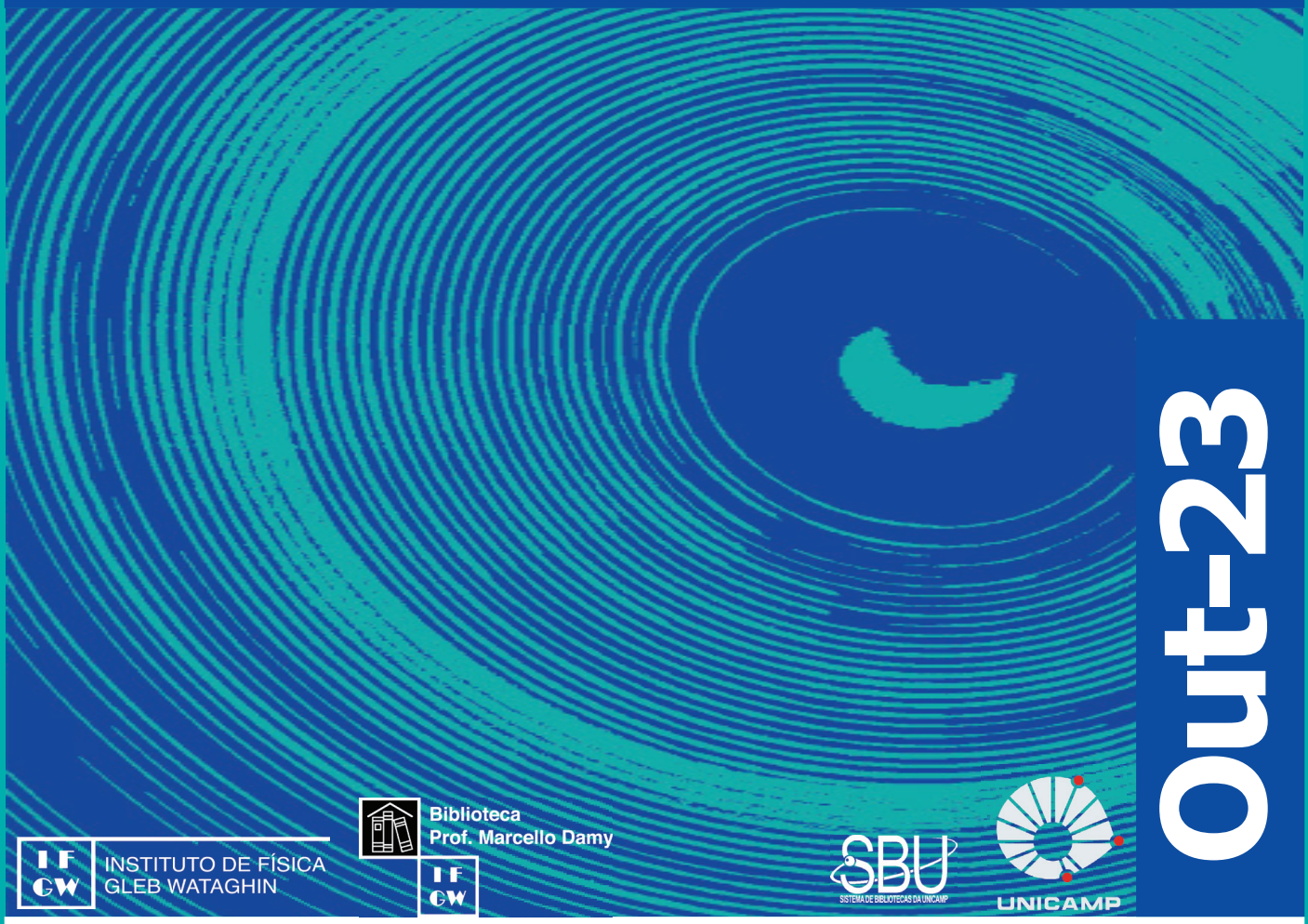

Out-23

INSTITUTO DE FÍSICA GLEB WATAGHIN

Biblioteca Prof. Marcello Damy

SBU SISTEMA DE BIBLIOTECAS DA UNICAMP

UNICAMP

Artigos publicados

[P154-2023] "2D Hemiporphyrazine: A new nanoporous material"

Tromer, R. M.*; Pereira, M. L.; Ribeiro, L. A.; **Galvao, D. S.***

Crystalline microporous materials are solids formed by interconnected pores of less than 2 nm in size. Typically, they possess large surface areas desirable for versatile applications such as catalysis, gas adsorption, and energy storage. In the present work, we propose a new porphyrin-based 2D nanoporous crystal, named 2D Hemiporphyrazine (2DH), which is formed by topologically assembling H5C13N4 porphyrins. We have considered its monolayer, bi-layer, and molecular crystal (bulk) arrangements. We carried out DFT calculations to investigate 2DH structural and electronic properties. Results show that 2DH is a very stable structure with a direct bandgap of 0.65 eV and significant optical absorption in the visible range. Simulations also showed the existence of proton transfer between nitrogen atoms. It is the first report on the site-specific hydrogen exchange process in 2D crystals.

PHYSICA E-LOW-DIMENSIONAL SYSTEMS & NANOSTRUCTURES 150, 115705, 2023. DOI: 10.1016/j.physe.2023.115705

[P155-2023] "3D-printed electrochemical cells with laser engraving: developing portable electroanalytical devices for forensic applications"

Matias, T. A.; Ramos, D. L. O.; Faria, L. V.; **Siervo, A. de***; Richter, E. M.; Munoz, R. A. A.

A new electrochemical device fabricated by the combination of 3D printing manufacturing and laser-generated graphene sensors is presented. Cell and electrodes were 3D printed by the fused deposition modeling (FDM) technique employing acrylonitrile butadiene styrene filament (insulating material that composes the cell) and conductive filament (lab-made filament based on graphite dispersed into polylactic acid matrix) to obtain reference and auxiliary electrodes. Infrared-laser engraved graphene, also reported as laser-induced graphene (LIG), was produced by laser conversion of a polyimide substrate, which was assembled in the 3D- printed electrochemical cell that enables the analysis of low volumes (50-2000 mu L). XPS analysis revealed the formation of nitrogen-doped graphene multilayers that resulted in excellent electrochemical sensing properties toward the detection of atropine (ATR), a substance that was found in beverages to facilitate sexual assault and other criminal acts. Linear range between 5 and 35 mu mol L-1, detection limit of 1 mu mol L-1, and adequate precision (RSD = 4.7%, n = 10) were achieved using differential-pulse voltammetry. The method was successfully applied to beverage samples with recovery values ranging from 80 to 105%. Interference studies in the presence of species commonly found in beverages confirmed satisfactory selectivity for ATR sensing. The devices proposed are useful portable analytical tools for on- site applications in the forensic scenario.

MICROCHIMICA ACTA 190[8], 297, 2023. DOI: 10.1007/s00604-023-05872-2

[P156-2023] "Agar-based optical sensors for electric current measurements"

Fujiwara, E.; Rosa, L. O.; Oku, H.; **Cordeiro, C. M. B.***

Biodegradable optical waveguides are breakthrough technologies to light delivery and sensing in biomedical and environmental applications.Agar emerges as an edible, soft, low-cost, and renewable alternative to traditional biopolymers, presenting remarkable optical and mechanical characteristics. Previous works introduced agar-made optical fibers for chemical measurements based on their inherent response to humidity and surrounding concentration. Therefore, we propose, for the first time, an all-optical, biodegradable electric current sensor. As flowing charges heat the agar matrix and modulate its refractive index, we connect the optical device to a DC voltage source using pin headers and excite the agar sample with coherent light to project spatiotemporally deviating speckle fields. Experiments proceeded with spheres and no-core fibers comprising 2 wt% agar/water. Once the increasing current stimulates the speckles' motion, we acquire such images with a camera and evaluate their correlation coefficients, yielding exponential decay-like functions whose time constants provide the input amperage. Furthermore, the light granules follow the polarization of the applied voltage drop, providing visual information about the current direction. The results indicate a maximum resolution of similar to 0.4 mu A for electrical stimuli <= 100 mu A, which fulfills the requirements for bioelectrical signal assessment.

SCIENTIFIC REPORTS 13[1], 13517, 2023. DOI: 10.1038/s41598-023-40749-7

[P157-2023] "Anisotropic flow and flow fluctuations of identified hadrons in Pb-Pb collisions at root(NN)-N-s=5.02 TeV"

Acharya, S.; Adamova, D.; **Chinellato, D. D.*; Guardiano, G. G.*; Jahnke, C.*; Takahashi, J.***; et al.
ALICE Collaboration

The first measurements of elliptic flow of pi(+/-), K-+/-, p+(p) over bar, K-S(0), Lambda + (Lambda) over bar, phi, Xi(-)+ Xi(+), and Omega(-) + (Omega) over bar (+) using multiparticle cumulants in Pb-Pb collisions at root(NN)-N-s = 5.02TeV are presented. Results obtained with two- (v2{2}) and four-particle cumulants (v(2){4}) are shown as a function of transverse momentum, pT, for various collision centrality intervals. Combining the data for both v(2){2} and v(2){4} also allows us to report the first measurements of the mean elliptic flow, elliptic flow fluctuations, and relative elliptic flow fluctuations for various hadron species. These observables probe the event--by-event eccentricity fluctuations in the initial state and the contributions from the dynamic evolution of the expanding quark-gluon plasma. The characteristic features observed in previous pT-differential anisotropic flow measurements for identified hadrons with two-particle correlations, namely the mass ordering at low pT and the approximate scaling with the number of constituent quarks at intermediate pT, are similarly present in the four-particle correlations and the combinations of v(2){2} and v(2){4}. In addition, a particle species dependence of flow fluctuations is observed that could indicate a significant contribution from final state hadronic interactions. The comparison between experimental measurements and CoLBT model calculations, which combine the various physics processes of hydrodynamics, quark coalescence, and jet fragmentation, illustrates their importance over a wide pT range.

JOURNAL OF HIGH ENERGY PHYSICS [5], 243, 2023. DOI: 10.1007/JHEP05(2023)243

[P158-2023] "Annealing effects on the magnetic and magnetotransport properties of iron oxide nanoparticles self--assemblies"

Fabris, F.*; Lima, E.; Nunez, J. M.; Troiani, H. E.; Aguirre, M. H.; Leboran, V.; Rivadulla, F.; Winkler, E. L.

In magnetic tunnel junctions based on iron oxide nanoparticles the disorder and the oxidation state of the surface spin as well as the nanoparticles functionalization play a crucial role in the magnetotransport properties.

In this work, we report a systematic study of the effects of vacuum annealing on the structural, magnetic and transport properties of self-assembled & SIM;10 nm Fe3O4 nanoparticles. The high temperature treatment (from 573 to 873 K) decomposes the organic coating into amorphous carbon, reducing the electrical resistivity of the assemblies by 4 orders of magnitude. At the same time, the 3.Fe2+/(Fe3++Fe2+) ratio is reduced from 1.11 to 0.13 when the annealing temperature of the sample increases from 573 to 873 K, indicating an important surface oxidation. Although the 2 nm physical gap remains unchanged with the thermal treatment, a monotonous decrease of tunnel barrier width was obtained from the electron transport measurements when the annealing temperature increases, indicating an increment in the number of defects and hot-spots in the gap between the nanoparticles. This is reflected in the reduction of the spin dependent tunneling, which reduces the interparticle magnetoresistance. This work shows new insights about influence of the nanoparticle interfacial composition, as well their the spatial arrangement, on the tunnel transport of self-assemblies, and evidence the importance of optimizing the nanostructure fabrication for increasing the tunneling current without degrading the spin polarized current.

NANOTECHNOLOGY 34[45], 455702, 2023. DOI: 10.1088/1361-6528/aced0e

[P159-2023] "Beyond Universal Volume Scaling: Tailoring Two-Photon Absorption in Nanomaterials by Heterostructure Design"

Alo, A.*; Barros, L. W. T.*; Nagamine, G.*; Lemus, J. C.*; Planelles, J.; Movilla, J. L.; Climente, J. I.; Lee, H. J.; Bae, W. K.; **Padilha, L. A.***

Colloidal semiconductor nanomaterials present broadband,with largecross-section, two-photon absorption (2PA) spectra, which turn theminto an important platform for applications that benefit from a highnonlinear optical response. Despite that, to date, the only meansto control the magnitude of the 2PA cross-section is by changing thenanoparticle volume, as it follows a universal volume scale, independentof the material composition. As the emission spectrum is connectedutterly to the nanomaterial dimensions, for a given material, themagnitude of the nonlinear optical response is also coupled to theemission spectra. Here, we demonstrate a means to decouple both effectsby exploring the 2PA response of different types of heterostructures,tailoring the volume dependence of the 2PA cross-section due to thedifferent dependence of the density of final states on the nanoparticlevolume. By heterostructure engineering, one can obtain 1 order ofmagnitude enhancement of the 2PA cross-section with minimum emissionspectra shift.

NANO LETTERS 23[15], 7180-7187, 2023. DOI: 10.1021/acs.nanolett.3c02131

[P160-2023] "Constraining the (K)over-barN coupled channel dynamics using femtoscopic correlations at the LHC"

Acharya, S.; Adamova, D.; **Chinellato, D. D.*; Guardiano, G. G.*; Jahnke, C.*; Takahashi, J.***; et al.
ALICE Collaboration

The interaction of K(-)with protons is characterised by the presence of several coupled channels, systems like (K) over bar (0)n and pi Sigma with a similar mass and the same quantum numbers as the K(-)p state. The strengths of these couplings to the K(-)p system are of crucial importance for the understanding of the nature of the Lambda(1405) resonance and of the attractive K(-)p strong interaction. In this article, we present measurements of the K(-)p correlation functions in relative momentum space obtained in pp collisions at root s = 13 Te, in p-Pb collisions at root sNN = 5.02 Te, and (semi)peripheral Pb-Pb collisions at root sNN = 5.02 Te. The emitting source size, composed of a core radius anchored to the K(+)p correlation and of a resonance halo specific to each particle pair, varies between 1 and 2 fm in these collision systems. The strength and the effects of the (K) over bar (0)n and pi Sigma inelastic channels on the measured K(-)p correlation function are investigated in the different colliding systems by comparing the data with state-of-the-art models of chiral potentials. A novel approach to determine the conversion weights omega, necessary to quantify the amount of produced inelastic channels in the correlation function, is presented. In this method, particle yields are estimated from thermal model predictions, and their kinematic distribution from blast-wave fits to measured data. The comparison of chiral potentials to the measured K(-)p interaction indicates that, while the pi Sigma-K(-)p dynamics is well reproduced by the model, the coupling to the (K) over bar (0)n channel in the model is currently underestimated.

EUROPEAN PHYSICAL JOURNAL C 83[4], 340, 2023. DOI: 10.1140/epjc/s10052-023-11476-0

[P161-2023] "Constraining the sources of ultra-high-energy cosmic rays across and above the ankle with the spectrum and composition data measured at the Pierre Auger Observatory"

Halim, A. A.; Abreu, P.; **Arbeletche, L. B.*; Chinellato, J. A.*; Franco, D. de O.*; Dobrigkeit, C.*; Fauth, A. C.*; Payeras, A. M.***; et al.
Pierre Auger Collaboration

In this work we present the interpretation of the energy spectrum and mass composition data as measured by the Pierre Auger Collaboration above 6x1017 eV. We use an astrophysical model with two extragalactic source populations to model the hardening of the cosmic-ray flux at around 5x1018 eV (the so-called "ankle" feature) as a transition between these two components. We find our data to be well reproduced if sources above the ankle emit a mixed composition with a hard spectrum and a low rigidity cutoff. The component below the ankle is required to have a very soft spectrum and a mix of protons and intermediate-mass nuclei. The origin of this intermediate-mass component is not well constrained and it could originate from either Galactic or extragalactic sources. To the aim of evaluating our capability to constrain astrophysical models, we discuss the impact on the fit results of the main experimental systematic uncertainties and of the assumptions about quantities affecting the air shower development as well as the propagation and redshift distribution of injected ultra-high-energy cosmic rays (UHECRs).

JOURNAL OF COSMOLOGY AND ASTROPARTICLE PHYSICS [5], 024, 2023. DOI: 10.1088/1475-7516/2023/05/024

[P162-2023] "Controllable Fano-type optical response and four-wave mixing via magnetoelastic coupling in an opto--magnomechanical system"

Sohail, A.; Ahmed, R.; Peng, J. X.; Munir, T.; Shahzad, A.; Singh, S. K.; **Oliveira, M. C. de***

We analytically investigate the Fano-type optical response and the four-wave mixing (FWM) process by exploiting the magnetoelasticity of a ferromagnetic material. The deformation of the ferromagnetic material plays the role of mechanical displacement, which is simultaneously coupled to both optical and magnon modes. We report that the magnetostrictively induced displacement leads to realization of Fano profiles in the output field and is effectively well-tuned through adjusting the system parameters, such as effective magnomechanical coupling,

magnon detuning, and cavity detuning. It is found that the magnetoelastic interaction also gives rise to the FWM phenomenon. The number of the FWM signals mainly depends upon the effective magnomechanical coupling and the magnon detuning. Moreover, the FWM spectrum exhibits suppressive behavior upon increasing (decreasing) the magnon (cavity) decay rate. The present scheme will open new perspectives in highly sensitive detection and quantum information processing.

JOURNAL OF APPLIED PHYSICS 133[15], 154401, 2023. DOI: 10.1063/5.0133156

[P163-2023] "Copper oxide nanostructures with nanoneedles shape obtained by direct reaction with nitrogen-doped carbon quantum dots: development of an electrochemical sensor to glyphosate"

Tiba, D. Y.; Name, L. L.; **Landers, R.***; Canevari, T. C.

This work describes the synthesis, characterization, and application of nanoneedle-shaped CuONPS/Cdot(N) nanostructures obtained by direct reaction between Cu(NO3)(2) and nitrogen--doped carbon quantum dots (Cdot(N)). The CDot(N) obtained from oleylamine using the electrochemical technique of chronoamperometry was used as catalysts and directing agents in synthesizing CuONPS/Cdot(N) nanostructures. The CuONPS/Cdot(N) nanostructures were characterized using transmission electron microscopy (HR-TEM), X-ray photoelectron spectroscopy (XPS), ultraviolet spectroscopy (UV-Vis), infrared spectroscopy (FTIR), and electrochemical techniques. HR-TEM and XPS analysis has shown that CuONPS/Cdot(N) nanostructures are constituted for both CuO and Cu2O nanospecies. The printed carbon electrode was modified with CuONPS/Cdot(N) nanostructures. It was used to determine the pesticide glyphosate in PBS, pH 5.5, at a potential of E = - 0.02 V, using the differential pulse voltammetry technique with a detection limit of 11.6 nMol L-1. The printed carbon electrode was modified with CuNPS/Cdot(N) nanostructures and was also used to determine pesticides in real water samples with good performance.

JOURNAL OF MATERIALS SCIENCE 58[31], 12569-12583, 2023. DOI: 10.1007/s10853-023-08827-3

[P164-2023] "Dark Energy Survey Year 3 results: Constraints on extensions to Lambda CDM with weak lensing and galaxy clustering"

Abbott, T. M. C.; Aguena, M.; **Brandao-Souza, A.*; Navarro--Alsina, A.*;** et al.
DES Collaboration

We constrain six possible extensions to the. cold dark matter (CDM) model using measurements from the Dark Energy Survey's first three years of observations, alone and in combination with external cosmological probes. The DES data are the two-point correlation functions of weak gravitational lensing, galaxy clustering, and their cross-correlation. We use simulated data vectors and blind analyses of real data to validate the robustness of our results to astrophysical and modeling systematic errors. In many cases, constraining power is limited by the absence of theoretical predictions beyond the linear regime that are reliable at our required precision. The.CDM extensions are dark energy with a time-dependent equation of state, nonzero spatial curvature, additional relativistic degrees of freedom, sterile neutrinos with eV-scale mass, modifications of gravitational physics, and a binned s 8ozTHORN model which serves as a phenomenological probe of structure growth. For the time-varying dark energy equation of state evaluated at the pivot redshift we find (w(p), w(a)) = (-0.99(-0.17)(+0.28), -0.9 +/- 1.2) at 68% confidence with z(p) = 0.24 from the DES measurements alone, and (w(p), w(a)) = (-1.03(-0.03)(+0.04), -0.4(-0.3)(+0.4)) with z(p) = 0.21 for the combination of all data considered. Curvature constraints of Omega(k) = 0.0009 +/- 0.0017 and effective relativistic species N-eff = 3.10(-0.16)(+0.15) are dominated by external data, though adding DES information to external low-redshift probes tightens the Omega(k) constraints that can be made without cosmic microwave background observables by 20%. For massive sterile neutrinos, DES combined with external data improves the upper bound on the mass m(eff) by a factor of 3 compared to previous analyses, giving 95% limits of (Delta N-eff, m(eff)) <= (0.28, 0.20 eV) when using priors matching a comparable Planck analysis. For modified gravity, we constrain changes to the lensing and Poisson equations controlled by functions Sigma(k, z) = Sigma(0)Omega(Lambda)(z)/Omega(Lambda,0) and mu(k,z) = mu(0)Omega(Lambda)(z)/Omega(Lambda,0), respectively, to Sigma(0) = 0.6(-0.5)(+0.4) from DES alone and (Sigma(0),mu(0)) = (0.04 +/- 0.05, 0.08(-0.19)(+0.21)) for the combination of all data, both at 68% confidence. Overall, we find no significant evidence for physics beyond Lambda CDM.

PHYSICAL REVIEW D 107[8], 083504, 2023. DOI: 10.1103/PhysRevD.107.083504

[P165-2023] "Dark Energy Survey Year 3 results: magnification modelling and impact on cosmological constraints from galaxy clustering and galaxy-galaxy lensing"

Elvin-Poole, J.; MacCrann, N. **Navarro-Alsina, A.***; et al.
DES Collaboration

We study the effect of magnification in the Dark Energy Survey Year 3 analysis of galaxy clustering and galaxy-galaxy lensing, using two different lens samples: a sample of luminous red galaxies, redMaGiC, and a sample with a redshift-dependent magnitude limit, MagLim. We account for the effect of magnification on both the flux and size selection of galaxies, accounting for systematic effects using the Balrog image simulations. We estimate the impact of magnification on the galaxy clustering and galaxy-galaxy lensing cosmology analysis, finding it to be a significant systematic for the MagLim sample. We show cosmological constraints from the galaxy clustering autocorrelation and galaxy-galaxy lensing signal with different magnifications priors, finding broad consistency in cosmological parameters in ?CDM and wCDM. However, when magnification bias amplitude is allowed to be free, we find the two-point correlation functions prefer a different amplitude to the fiducial input derived from the image simulations. We validate the magnification analysis by comparing the cross-clustering between lens bins with the prediction from the baseline analysis, which uses only the autocorrelation of the lens bins, indicating that systematics other than magnification may be the cause of the discrepancy. We show that adding the cross-clustering between lens redshift bins to the fit significantly improves the constraints on lens magnification parameters and allows uninformative priors to be used on magnification coefficients, without any loss of constraining power or prior volume concerns.

MONTHLY NOTICES OF THE ROYAL ASTRONOMICAL SOCIETY 523[3], 3649-3670, 2023. DOI: 10.1093/mnras/stad1594

[P166-2023] "Electron ionization induced fragmentation pathways of trichloroanisole"

Mendes, M.; Bou-Debes, D.; Eden, S.; Bundaleski, N.; Teodoro, O. M. N. D.; **Cornetta, L. M.*;** Silva, F. F. da

Trichloroanisole (TCA) is one of the most significant contaminants in cork stoppers. The presence of TCA leads to an unpleasant odor known as "cork taint", resulting in high economic losses for the cork and wine industries. Hence, the detection, quantification, and characterization of TCA are essential to address this concern.

The present study investigates the electron-driven fragmentation pathways of TCA through electron ionization mass spectrometry as a function of electron energy (0-100 eV), and the results are supported by theoretical characterization of ionization potentials, dissociation thresholds, and electron ionization cross sections. The appearance energies of ten cations were measured, including the first experimental evaluation of the molecule's ionization energy at 8.8 & PLUSMN; 0.3 eV, in excellent agreement with the calculations (8.83 eV). For lower energies, around 20 eV, the parent cation accounted for more than 60% of the total ion signal, followed by its demethylated fragment. Taken together, these ion signals could be used as fingerprints of TCA in industrial quality control by low-energy electron ionization mass spectrometry. Fifty other fragments have been identified at higher electron energies, revealing the very rich fragmentation pattern of TCA. This work probes electron-driven ionization of TCA. New fragment ions are identified by mass spectrometry and experimental appearance energies show excellent agreement with calculated threshold energies for the most significant pathways.

PHYSICAL CHEMISTRY CHEMICAL PHYSICS, 2023. DOI: 10.1039/d3cp02019 **Primeira data de acesso:** AUG 2023

[P167-2023] "Electronic structure of Co 3d states in the Kitaev material candidate honeycomb cobaltate Na3Co2SbO6 probed with x-ray dichroism"

Autor(es): van Veenendaal, M.; Poldi, E. H. T.; Veiga, L. S. I.; Bencok, P.; Fabbris, G.; **Tartaglia, R.***; Mcchesney, J. L.; Freeland, J. W.; Hemley, R. J.; Zheng, H.; Mitchell, J. F.; Yan, J. Q.; Haskel, D.

The recent prediction that honeycomb lattices of Co2+ (3d7) ions could host dominant Kitaev interactions provides an exciting direction for exploration of new routes to stabilizing Kitaev's quantum spin liquid in real materials. Na3Co2SbO6 has been singled out as a potential material candidate provided that spin and orbital moments couple into a Jeff = 12 ground state, and that the relative strength of trigonal crystal field and spin-orbit coupling acting on Co ions can be tailored. Using x-ray linear dichroism (XLD) and x-ray magnetic circular dichroism (XMCD) experiments, alongside configuration interaction calculations, we confirm the counterintuitive positive sign of the trigonal crystal field acting on Co2+ ions and test the validity of the Jeff = 12 description of the electronic ground state. The results lend experimental support to recent theoretical predictions that a compression (elongation) of CoO6 octahedra along (perpendicular to) the trigonal axis would drive this cobaltate toward the Kitaev limit, assuming the Jeff = 12 character of the electronic ground state is preserved.

PHYSICAL REVIEW B 107[21], 214443, 2023. DOI: 10.1103/PhysRevB.107.214443

[P168-2023] "Energy harvesting using two-dimensional magnesiochromite (MgCr2O4)"

Mahapatra, P. L.; Singh, A. K.; **Tromer, R.***; Kumbhakar, P.; Sinha, S. K.; Lahiri, B.; Kundu, T. K.; **Galvao, D. S.***; Tiwary, C. S.

Two-dimensional (2D) materials with high surface activity can be utilized for harvesting energy from small mechanical sources using flexoelectricity. In the present work, we have synthesized an atomically thin 2D spinel MgCr2O4 by a liquid-phase exfoliation process, and characterization shows the preferential exfoliation along the (111) plane with low formation energy. The fabricated flexoelectric device produces an electrical response up to-3 V (peak-to-peak voltage) upon pressing and releasing the cell with-0.98 N force. Furthermore, the energy harvesting properties of 2D MgCr2O4 are explored by combining bending with other sources of external energy, with applied varying magnetic flux (Vmax 1/4-2.6 V) and temperature with 0.9 N force (Vmax 1/4-18 V). Our calculations determine that 2D MgCr2O4 has a flexoelectric coefficient of approximately mXZXZ 1/4 0.005 nC/m. Overall, the results indicate that 2D MgCr2O4 is a very promising material for the next generation of self-powered wearable electronics and energy harvesting.

MATERIALS TODAY NANO 23, 100374, 2023. DOI: 10.1016/j.mtnano.2023.100374

[P169-2023] "Enhancing nonclassical properties of quantum states of light using linear optics"

Mattos, E. P.*; Vidiella-Barranco, A.*

In this Letter, we present a simple and versatile scheme for enhancing the nonclassical properties of light states using only linear optics and photodetectors. By combining a coherent state |& alpha;) and an arbitrary pure state of light |& phi;) (excluding coherent states) at two beam splitters, we show that the amplitude & alpha; of the coherent state can be tuned to filter out specific Fock components and generate states of light with increased nonclassical features. We provide two examples of input states and demonstrate the effectiveness of our scheme in enhancing the sub-Poissonian statistics or the quadrature squeezing of the output states.

OPTICS LETTERS 48[14], 3645-3648, 2023. DOI: 10.1364/OL.494609

[P170-2023] "Equilibrium of longitudinal bunch distributions in electron storage rings with arbitrary impedance sources and generic filling patterns"

Alves, M. B.*; Sa, F. H. de

A new self-consistent semianalytical method for calculating the stationary beam-induced voltage in the presence of arbitrary filling patterns and impedance sources in electron storage rings is presented. The theory was developed in space domain with resonator wake functions and in frequency domain with arbitrary impedance functions. The SIRIUS storage ring parameters were used to benchmark the results, demonstrating good agreement between the two approaches and with macroparticle tracking simulations. Additionally, a different approach to simulate the beam-loading compensation of active rf cavities was investigated in frequency domain, proving to be a more generic description than the methods generally used. The impact of broadband impedance on the longitudinal equilibrium was straightforwardly evaluated with the frequency-domain framework, without intermediate steps such as fitting broadband resonators or convolving short-range wakes with bunch distributions. Finally, a simple study of Touschek's lifetime improvement with a passive higher harmonic cavity is presented.

PHYSICAL REVIEW ACCELERATORS AND BEAMS 26[9], 094402, 2023. DOI: 10.1103/PhysRevAccelBeams.26.094402

[P171-2023] "Explicit parametrization of more than one vectorlike quark of Nelson-Barr type"

Alves, G. H. S.; **Cherchiglia, A. L.*;** Nishi, C. C.

Nelson-Barr models solve the strong CP problem based on spontaneous CP violation and generically require vectorlike quarks (VLQs) mixing with standard quarks to transmit the CP violation.

We devise an explicit parametrization for the case of two VLQs of either down or up type and quantitatively study several aspects including the hierarchy of the VLQ Yukawas and their irreducible contribution to & theta; over bar . In particular, with the use of the parametrization, we show that a big portion of the parameter space for two up-type VLQs at the TeV scale is still allowed by the constraint on & theta; over bar , although this case had been previously shown to be very restricted based on estimates.

PHYSICAL REVIEW D 108[3], 035049, 2023. DOI: 10.1103/PhysRevD.108.035049

[P172-2023] "Exploring the elastic properties and fracture patterns of Me-graphene monolayers and nanotubes through reactive molecular dynamics simulations"

Pereira Junior, M. L.; **Sousa, J. M. de***; Brandao, W. H. S.; **Galvao, D. S.***; **Fonseca, A. F.***; Junior, L. A. R.

Me-graphene (MeG) is a novel two-dimensional (2D) carbon allotrope. Due to its attractive electronic and structural properties, it is important to study the mechanical behavior of MeG in its monolayer and nanotube topologies. In this work, we conducted fully atomistic reactive molecular dynamics simulations using the Tersoff force field to investigate their mechanical properties and fracture patterns. Our results indicate that Young's modulus of MeG monolayers is about 414 GPa and in the range of 421-483 GPa for the nanotubes investigated here. MeG monolayers and MeGNTs directly undergo from elastic to complete fracture under critical strain without a plastic regime.

CHEMICAL PHYSICS LETTERS 830, 140812, 2023. DOI: 10.1016/j.cplett.2023.140812

[P173-2023] "First measurement of Lambda(+)(c) production down to p(T)=0 in pp and p-Pb collisions at root s(NN)=5.02 TeV"

Acharya, S.; Adamova, D.; **Chinellato, D. D.***; **Guardiano, G. G.***; **Jahnke, C.***; **Takahashi, J.***; et al.
ALICE Collaboration

The production of prompt Lambda(+)(c) baryons has been measured at midrapidity in the transverse momentum interval 0 < pT < 1 GeV/c for the first time, in pp and p-Pb collisions at a center-of-mass energy per nucleon-nucleon collision root s(NN) = 5.02 TeV. The measurement was performed in the decay channel Lambda(+)(c) . pK0 S by applying new decay reconstruction techniques using a Kalman-Filter vertexing algorithm and adopting a machine-learning approach for the candidate selection. The pT -integrated Lambda(+)(c) production cross sections in both collision systems were determined and used along with the measured yields in Pb-Pb collisions to compute the pT -integrated nuclear modification factors RpPb and RAA of Lambda(+)(c) baryons, which are compared to model calculations that consider nuclear modification of the parton distribution functions. The Lambda(+)(c) /D0 baryon-to-meson yield ratio is reported for pp and p-Pb collisions. Comparisons with models that include modified hadronization processes are presented, and the implications of the results on the understanding of charm hadronization in hadronic collisions are discussed. A significant (3.7s) modification of the mean transverse momentum of Lambda(+)(c) baryons is seen in p-Pb collisions with respect to pp collisions, while the pT -integrated Lambda(+)(c) /D0 yield ratio was found to be consistent between the two collision systems within the uncertainties.

PHYSICAL REVIEW C 107[6], 064901, 2023. DOI: 10.1103/PhysRevC.107.064901

[P174-2023] "Fluorescence Spectroscopy: from Fundamentals to the Influence of Instrumental Parameters for Analysis of Organic dyes and Inorganic Nanoparticles"

Mourao, R. S.; **Vale, B. R. C.***; Fonseca, A. F. V.; **Carvalho, T. A. S.***; Schiavon, M. A.

Fluorescence spectroscopy is an extremely sensitive analytical technique that has been widely used to elucidate problems that require low detection limits. Although fluorescence spectroscopy is widespread in industry and academia, there is a lack of teaching materials demonstrating its basic principles, as well as the influence of instrumental parameters involved in the technique, which limit its correct use and the full potential of it. For this reason, this work aims to explore the principles of fluorescence spectroscopy and correlate them in function of different instrumental variables to carry out a fluorescence experiment. The spectrofluorometer parameters such as the excitation wavelength, excitation and emission slits, step, integration time, detection geometry as well as concentration of the samples were varied to illustrate how the best resulting spectra can be registered free of artifacts. To do so, two organic dyes with structured vibronic bands (pyrene) and another with unstructured bands (rhodamine 6G) were used. Another study carried out involved the use of 3D spectra, excitation/emission spectra, of cadmium telluride (CdTe) quantum dots. In this case, it was possible to show the excitation spectrum of nanomaterials, collecting emissions at different wavelengths, as well as analyzing the particle size distribution.

QUIMICA NOVA, 2023. DOI: 10.21577/0100-4042.20230095
Primeira data de acesso: AUG 2023

[P175-2023] "Impact of cross-section uncertainties on supernova neutrino spectral parameter fitting in the Deep Underground Neutrino Experiment"

Abud, A. A.; Abi, B.; **Adriano, C.***; **Bazetto, M. C. Q.***; **Aguiar, R. de***; **Almeida, P. de***; **Holanda, P. C. de***; **Souza, G. de***; **Gelli, B.***; **Giammaria, P.***; **Guzzo, M. M.***; **Kemp, E.***; **Machado, A. A.***; **Peres, O. L. G.***; **Pimentel, V. L.***; **Prakash, S.***; **Ratoff, P.***; **Segreto, E.***; et al.
DUNE Collaboration

A primary goal of the upcoming Deep Underground Neutrino Experiment (DUNE) is to measure the Oo10 thorn MeV neutrinos produced by a Galactic core-collapse supernova if one should occur during the lifetime of the experiment. The liquid-argon--based detectors planned for DUNE are expected to be uniquely sensitive to the & nu;e component of the supernova flux, enabling a wide variety of physics and astrophysics measurements. A key requirement for a correct interpretation of these measurements is a good understanding of the energy-dependent total cross section & sigma;oE & nu; thorn for charged-current & nu;e absorption on argon. In the context of a simulated extraction of supernova & nu;e spectral parameters from a toy analysis, we investigate the impact of & sigma;oE & nu; thorn modeling uncertainties on DUNE's supernova neutrino physics sensitivity for the first time. We find that the currently large theoretical uncertainties on & sigma;oE & nu; thorn must be substantially reduced before the & nu;e flux parameters can be extracted reliably; in the absence of external constraints, a measurement of the integrated neutrino luminosity with less than 10% bias with DUNE requires & sigma;oE & nu; thorn to be known to about 5%. The neutrino spectral shape parameters can be known to better than 10% for a 20% uncertainty on the cross--section scale, although they will be sensitive to uncertainties on the shape of & sigma;oE & nu; thorn . A direct measurement of low-energy & nu;e-argon scattering would be invaluable for improving the theoretical precision to the needed level.

PHYSICAL REVIEW D 107[11], 112012, 2023. DOI: 10.1103/PhysRevD.107.112012

[P176-2023] "Indirect effects shape species fitness in coevolved mutualistic networks"

Cosmo, L. G.; Assis, A. P. A.; **Aguiar, M. A. M. de***; Pires, M. M.; Valido, A.; Jordano, P.; Thompson, J. N.; Bascompte, J.; Guimaraes Jr., P.

Ecological interactions are one of the main forces that sustain Earth's biodiversity. A major challenge for studies of ecology and evolution is to determine how these interactions affect the fitness of species when we expand from studying isolated, pairwise interactions to include networks of interacting species(1-4). In networks, chains of effects caused by a range of species have an indirect effect on other species they do not interact with directly, potentially affecting the fitness outcomes of a variety of ecological interactions (such as mutualism)(5-7). Here we apply analytical techniques and numerical simulations to 186 empirical mutualistic networks and show how both direct and indirect effects alter the fitness of species coevolving in these networks. Although the fitness of species usually increased with the number of mutualistic partners, most of the fitness variation across species was driven by indirect effects. We found that these indirect effects prevent coevolving species from adapting to their mutualistic partners and to other sources of selection pressure in the environment, thereby decreasing their fitness. Such decreases are distributed in a predictable way within networks: peripheral species receive more indirect effects and experience higher reductions in fitness than central species. This topological effect was also evident when we analysed an empirical study of an invasion of pollination networks by honeybees. As honeybees became integrated as a central species within networks, they increased the contribution of indirect effects on several other species, reducing their fitness. Our study shows how and why indirect effects can govern the adaptive landscape of species-rich mutualistic assemblages.

NATURE, 2023. DOI: 10.1038/s41586-023-06319-7, **Primeira data de acesso: J**UL 2023

[P177-2023] "Influence of Methylammonium Chloride on Wide-Bandgap Halide Perovskites Films for Solar Cells"

Guaita, M. G. D.; Szostak, R.; **Silva, F. M. C. da***; Morais, A. de; Moral, R. F.; Kodalle, T.; Teixeira, V. C.; Sutter-Fella, C. M.; Tolentino, H. C. N.; Nogueira, A. F.

Wide-bandgap perovskites are of paramount importance as the photoactive layer of the top cell in high-efficiency tandem solar cells. Comparably high Br contents are required to widen the perovskite bandgap. However, the increase in Br content causes heterogeneous halide distribution and photoinstability. Here, the positive effect of the additive methylammonium chloride (MACl) on the optical and electronic properties of Br-rich perovskite, deposited using N-methyl-2-pyrrolidone (NMP) as co-solvent and the gas quenching method, is investigated. Simultaneous in situ grazing-incidence wide-angle X-ray scattering and photoluminescence spectroscopy are used to track the evolution of the structural and optoelectronic properties of the perovskites with different amounts of Br and MACl during the spin-coating and thermal annealing steps. The formation mechanism is elucidated in the presence of MACl. It is observed that chloride ions inhibit the intermediate phases, favoring the formation of a perovskite phase with higher crystallinity. Nano X-ray fluorescence mapping recognizes Br-richer and poorer nanometric domains, whose average sizes reduce for samples with MACl. In conclusion, it is demonstrated that adding MACl affects the formation of wide-bandgap perovskites via destabilization of the intermediate phases and acts on the homogenization of the halide distribution, leading to improved solar cell performances. Wide-bandgap perovskites are relevant materials for tandem cells. However, the addition of bromine, to increase the bandgap, leads to the formation of a perovskite richer in defects, with halide distribution heterogeneity and photoinstability. Here, the study of the impact and mode of action of methylammonium chloride (MACl) additive, shows the inhibition of intermediates formation and the halide distribution homogenization with MACl.image

ADVANCED FUNCTIONAL MATERIALS, 2023. DOI: 10.1002/adfm.202307104, **Primeira data de acesso:** SEP 2023

[P178-2023] "Iron Oxide Nanoparticles in a Dynamic Flux: Magnetic Hyperthermia Effect on Flowing Heavy Crude Oil"

Brollo, M. E. F.*; Pinheiro, I. F.; Bassani, G. S.; Varet, G.; Merino-Garcia, D.; Guersoni, V. C. B.; **Knobel, M.***; Bannwart, A. C.; van der Geest, C.; **Muraca, D.***

An essential part for crude oil extraction is flow assurance, being critical to maintain a financially sustainable flow while getting the petroleum to the surface. When not well managed, it can develop into a significant issue for the O & G industry. By heating the fluids, problems with flow assurance, including paraffin deposition, asphaltene, and methane hydrate, can be reduced. Also, as the temperature rises, a liquid's viscosity decreases. Research focusing on the application of magnetic nanoparticles (NPs) in the oil industry is very recent. When magnetic nanofluids are exposed to an alternating magnetic field, the viscosity decreases by several orders of magnitude as a result of the fluid's temperature rising due to a phenomenon known as magnetic hyperthermia. This work focuses on the use of magnetic NPs (9 nm) in heavy crude oil (API 19.0). The frequency and strength of the magnetic field, as wel l as the characteristics of the fluid and the NPs intrinsic properties all affect the heating efficiency. For al l of the experimental settings in this work, the flowloop's temperature increased, reaching a maximum of ?T = 16.3 degrees C, using 1% wt NPs at the maximum available frequency of the equipment (533 kHz) and the highest field intensity for this frequency (14 kA/m), with a flow rate of 1.2 g/s. This increase in temperature causes a decrease of nearly 45% on the heavy crude oil viscosity, and if properly implemented, could substantially increase oil flow in the field during production.

ACS OMEGA 8[36], 32520-32525, 2023. DOI: 10.1021/acsomega.3c02832

[P179-2023] "J/ψ production at midrapidity in p-Pb collisions at √sNN=8.16 TeV"

Acharya, S.; Adamova, D.; **Chinellato, D. D.*; Guardiano, G. G.*; Jahnke, C.*; Takahashi, J.***; et al.
ALICE Collaboration

The production of inclusive, prompt and non-prompt J/psi was studied for the first time at midrapidity (-1.37 < y(cms) < 0.43) in p-Pb collisions at root sNN = 8.16 TeV with the ALICE detector at the LHC. The inclusive J/psi mesons were reconstructed in the dielectron decay channel in the transverse momentum (p(T)) interval 0 < p(T) < 14 GeV/ c and the prompt and non-prompt contributions were separated on a statistical basis for pT > 2 GeV/c. The study of the J/psi mesons in the dielectron channel used for the first time in ALICE online single-electron triggers from the Transition Radiation Detector, providing a data sample corresponding to an integrated luminosity of 689 +/- 13 mu b(-1). The proton-proton reference cross section for inclusive J/psi was obtained based on interpolations of measured data at different centre-of-mass energies and a universal function describing the p(T)-differential J/psi production cross sections. The p(T)-differential nuclear modification factors R-pPb of inclusive, prompt, and non-prompt J/psi are consistent with unity and described by theoretical models implementing only nuclear shadowing.

JOURNAL OF HIGH ENERGY PHYSICS [7], 137, 2023. DOI: 10.1007/JHEP07(2023)137

[P180-2023] "Kinematic Sunyaev-Zel'dovich effect with ACT, DES, and BOSS: A novel hybrid estimator"

Mallaby-Kay, M.; Amodeo, S.; **Sobreira, F.***; et al.

The kinematic and thermal Sunyaev-Zel'dovich (kSZ and tSZ) effects probe the abundance and thermodynamics of ionized gas in galaxies and clusters. We present a new hybrid estimator to measure the kSZ effect by combining cosmic microwave background temperature anisotropy maps with photometric and spectroscopic optical survey data. The method interpolates a velocity reconstruction from a spectroscopic catalog at the positions of objects in a photometric catalog, which makes it possible to leverage the high number density of the photometric catalog and the precision of the spectroscopic survey. Combining this hybrid kSZ estimator with a measurement of the tSZ effect simultaneously constrains the density and temperature of free electrons in the photometrically selected galaxies. Using the 1000 deg2 of overlap between the Atacama Cosmology Telescope (ACT) Data Release 5, the first three years of data from the Dark Energy Survey (DES), and the Baryon Oscillation Spectroscopic Survey (BOSS) Data Release 12, we detect the kSZ signal at 4.8 & sigma; and reject the null (no-kSZ) hypothesis at 5.1 & sigma;. This corresponds to 2.0 & sigma; per 100,000 photometric objects with a velocity field based on a spectroscopic survey with 1=5th the density of the photometric catalog. For comparison, a recent ACT analysis using exclusively spectroscopic data from BOSS measured the kSZ signal at 2.1 & sigma; per 100,000 objects. Our derived constraints on the thermodynamic properties of the galaxy halos are consistent with previous measure-ments. With future surveys, such as the Dark Energy Spectroscopic Instrument and the Rubin Observatory Legacy Survey of Space and Time, we expect that this hybrid estimator could result in measurements with significantly better signal--to-noise than those that rely on spectroscopic data alone.

PHYSICAL REVIEW D 108[2], 023516, 2023. DOI: 10.1103/PhysRevD.108.023516

[P181-2023] "Light (anti)nuclei production in Pb-Pb collisions at root s(NN)=5.02 TeV"

Acharya, S.; Adamova, D.; **Albuquerque, D. S. D.*; Chinellato, D. D.*; Takahashi, J.***; et al.
ALICE Collaboration

The measurement of the production of deuterons, tritons and 3He and their antiparticles in Pb-Pb collisions at & RADIC;sNN = 5.02 TeV is presented in this article. The measurements are carried out at midrapidity (|y| < 0.5) as a function of collision centrality using the ALICE detector. The pT-integrated yields, the coalescence parameters and the ratios to protons and antiprotons are reported and compared with nucleosynthesis models. The comparison of these results in different collision systems at different center-of-mass collision energies reveals a suppression of nucleus production in small systems. In the Statistical Hadronisation Model framework, this can be explained by a small correlation volume where the baryon number is conserved, as already shown in previous fluctuation analyses. However, a different size of the correlation volume is required to describe the proton yields in the same data sets. The coalescence model can describe this suppression by the fact that the wave functions of the nuclei are large and the fireball size starts to become comparable and even much smaller than the actual nucleus at low multiplicities.

PHYSICAL REVIEW C 107[6], 064904, 2023. DOI: 10.1103/PhysRevC.107.064904

[P182-2023] "Magnetic phase recognition of artificial kagome spin ice through initial magnetization curve"

Cecchi, B. M.*; Cruz, N.*; Knobel, M.*; Pirota, K. R.*

Artificial spin ices (ASIs) are designable arrays of interacting nanomagnets that span a wide range of magnetic phases. Here, we demonstrate that the phase of an artificial kagome spin ice can be identified through its initial magnetization curve. As a proof of concept, micromagnetic simulations of these curves were performed starting from representative microstates of different phases of the system. We show that the curves are characterized by phase-specific features in such a way that a supervised classification algorithm predicts the phase of the initial microstate with good reliability. Moreover, most curves associated with paramagnetic and spin ice 1 phases are recognizable simply by visual inspection. This achievement represents a different strategy for identifying phases in ASIs that is easier and more accessible than magnetic imaging techniques normally used for this task.

PHYSICAL REVIEW B 108[1], 014404, 2023. DOI: 10.1103/PhysRevB.108.014404

[P183-2023] "Measurement of (2S) production as a function of charged-particle pseudorapidity density in pp collisions at root s=13 TeV and p-Pb collisions at root s(NN)=8.16 TeV with ALICE at the LHC"

Acharya, S.; Adamova, D.; **Chinellato, D. D.*; Guardiano, G. G.*; Jahnke, C.*; Takahashi, J.*;** et al.
ALICE Collaboration

Production of inclusive charmonia in pp collisions at center-of--mass energy of root s = 13TeV and p-Pb collisions at center-of--mass energy per nucleon pair of root sNN = 8.16TeV is studied as a function of charged-particle pseudorapidity density with ALICE. Ground and excited charmonium states (J/psi, psi(2S)) are measured from their dimuon decays in the interval of rapidity in the center-of-mass frame 2.5 < y(cms) < 4.0 for pp collisions, and 2.03 < y(cms) < 3.53 and -4.46 < y(cms) < -2.96 for p-Pb collisions. The charged-particle pseudorapidity density is measured around midrapidity (| eta | < 1.0). In pp collisions, the measured charged-particle multiplicity extends to about six times the average value, while in p-Pb collisions at forward (backward) rapidity a multiplicity corresponding to about three (four) times the average is reached. The psi(2S) yield increases with the charged-particle pseudorapidity density. The ratio of psi(2S) over J/ yield does not show a significant multiplicity dependence in either colliding system, suggesting a similar behavior of J/ and psi(2S) yields with respect to charged-particle pseudorapidity density. Results for the psi(2S) yield and its ratio with respect to J/psi agree with available model calculations.

JOURNAL OF HIGH ENERGY PHYSICS [6], 147, 2023. DOI: 10.1007/JHEP06(2023)147

[P184-2023] "Measurement of inclusive and differential cross sections for single top quark production in association with a W boson in proton-proton collisions at √s=13TeV"

Tumasyan, A.; Adam, W.; **Chinellato, J. A.***; et al.
CMS Collaboration

Measurements of the inclusive and normalised differential cross sections are presented for the production of single top quarks in association with a W boson in proton-proton collisions at a centre-of-mass energy of 13TeV. The data used were recorded with the CMS detector at the LHC during 2016-2018, and correspond to an integrated luminosity of 138 fb(-1). Events containing one electron and one muon in the final state are analysed. For the inclusive measurement, a multivariate discriminant, exploiting the kinematic properties of the events is used to separate the signal from the dominant t (t) over bar background.

A cross section of 79.2 +/- 0.9 (stat)(-8.0)(+7.7) (syst) +/- 1.2 (lumi) pb is obtained, consistent with the predictions of the standard model. For the differential measurements, a fiducial region is defined according to the detector acceptance, and the requirement of exactly one jet coming from the fragmentation of a bottom quark. The resulting distributions are unfolded to particle level and agree with the predictions at next--to-leading order in perturbative quantum chromodynamics.

JOURNAL OF HIGH ENERGY PHYSICS [7], 46, 2023. DOI: 10.1007/JHEP07(2023)046

[P185-2023] "Measurement of inclusive and leading subjet fragmentation in pp and Pb-Pb collisions at root(NN)-N--s=5.02 TeV"

Acharya, S.; Adamova, D.; **Chinellato, D. D.*; Guardiano, G. G.*; Jahnke, C.*; Takahashi, J.***; et al.
ALICE Collaboration

This article presents new measurements of the fragmentation properties of jets in both proton-proton (pp) and heavy--ion collisions with the ALICE experiment at the Large Hadron Collider (LHC). We report distributions of the fraction z(r) of transverse momentum carried by subjets of radius r within jets of radius R. Charged-particle jets are reconstructed at midrapidity using the anti- kT algorithm with jet radius R = 0.4, and subjets are reconstructed by reclustering the jet constituents using the anti-k(T) algorithm with radii r = 0.1 and r = 0.2. In proton-proton collisions, we measure both the inclusive and leading subjet distributions. We compare these measurements to perturbative calculations at next-to-leading logarithmic accuracy, which suggest a large impact of threshold resummation and hadronization effects on the z(r) distribution. In heavy-ion collisions, we measure the leading subjet distributions, which allow access to a region of harder jet fragmentation than has been probed by previous measurements of jet quenching via hadron fragmentation distributions. The z(r) distributions enable extraction of the parton-to-subjet fragmentation function and allow for tests of the universality of jet fragmentation functions in the quark-gluon plasma (QGP). We find no significant modification of z(r) distributions in Pb-Pb compared to pp collisions. However, the distributions are also consistent with a hardening trend for zr < 0.95, as predicted by several jet quenching models. As z(r) -> 1 our results indicate that any such hardening effects cease, exposing qualitatively new possibilities to disentangle competing jet quenching mechanisms. By comparing our results to theoretical calculations based on an independent extraction of the parton-to-jet fragmentation function, we find consistency with the universality of jet fragmentation and no indication of factorization breaking in the QGP.

JOURNAL OF HIGH ENERGY PHYSICS [5], 245, 2023. DOI: 10.1007/JHEP05(2023)245

[P186-2023] "Measurement of the angle between jet axes in pp collisions at √s=5.02 TeV"

Acharya, S.; Adamova, D.; **Chinellato, D. D.*; Guardiano, G. G.*; Jahnke, C.*; Takahashi, J.***; et al.
ALICE Collaboration

This article reports measurements of the angle between differently defined jet axes in pp collisions at root s = 5.02TeV carried out by the ALICE Collaboration. Charged particles at midrapidity are clustered into jets with resolution parameters R = 0.2 and 0.4. The jet axis, before and after Soft Drop grooming, is compared to the jet axis from the Winner--Takes-All (WTA) recombination scheme. The angle between these axes, Delta R-axis, probes a wide phase space of the jet formation and evolution, ranging from the initial high--momentum-transfer scattering to the hadronization process. The Delta R-axis observable is presented for 20 < p(T)(ch jet) < 100 GeV/c, and compared to predictions from the PYTHIA 8 and Herwig 7 event generators. The distributions can also be calculated analytically with a leading hadronization correction related to the non-perturbative component of the Collins Soper-Sterman (CSS) evolution kernel. Comparisons to analytical predictions at nextto-leading-logarithmic accuracy with leading hadronization correction implemented from experimental extractions of the CSS kernel in Drell-Yan measurements are presented. The analytical predictions describe the measured data within 20% in the perturbative regime, with surprising agreement in the non-perturbative regime as well. These results are compatible with the universality of the CSS kernel in the context of jet substructure.

JOURNAL OF HIGH ENERGY PHYSICS [7], 201, 2023. DOI: 10.1007/JHEP07(2023)201

[P187-2023] "Measurement of the B-s(0) = mu(+)mu(-) decay properties and search for the B-0 -> mu(+)mu(-) decay in proton-proton collisions at root s=13 TeV"

Tumasyan, A.; Adam, W.; **Chinellato, J. A.***; et al.
CMS Collaboration

Measurements are presented of the B0s & RARR; & mu;+& mu;- branching fraction and effective lifetime, as well as results of a search for the B0 & RARR; & mu;+& mu;- decay in proton-proton collisions at & RADIC;s =13 TeV at the LHC. The analysis is based on data collected with the CMS detector in 2016-2018 corresponding to an integrated luminosity of 140 fb-1. The branching fraction of the B0s & RARR; & mu;+& mu;- decay and the effective B0s meson lifetime are the most precise single measurements to date. No evidence for the B0 & RARR; & mu;+& mu;- decay has been found. All results are found to be consistent with the standard model predictions and previous measurements. & COPY; 2023 The Author(s). Published by Elsevier B.V. This is an open access article under the CC BY license (http://creativecommons .org /licenses /by /4 .0/). Funded by SCOAP3.

PHYSICS LETTERS B 842, 137955, 2023. DOI: 10.1016/j.physletb.2023.137955

[P188-2023] "Measurement of the cross section of top quark-antiquark pair production in association with a W boson in proton-proton collisions at √s=13 TeV"

Tumasyan, A.; Adam, W.; **Chinellato, J. A.***; et al.
CMS Collaboration

The production of a top quark-antiquark pair in association with a W boson (t (t) over barW) is measured in proton-proton collisions at a center-of-mass energy of 13TeV. The analyzed data was recorded by the CMS experiment at the CERN LHC and corresponds to an integrated luminosity of 138 fb(-1). Events with two or three leptons (electrons and muons) and additional jets are selected. In events with two leptons, a multiclass neural network is used to distinguish between the signal and background processes. Events with three leptons are categorized based on the number of jets and of jets originating from b quark hadronization, and the lepton charges. The inclusive t (t) over barW(+) production cross section in the full phase space is measured to be 868 +/- 40(stat)+/- 51(syst) fb. The t (t) over barW(+) and t (t) over barW(-) cross sections are also measured as 553 +/- 30(stat)+/- 30(syst) and 343 +/- 26(stat)+/- 25(syst) fb, respectively, and the corresponding ratio of the two cross sections is found to be 1.61 +/- 0.15(stat)(-0.05)(+0.07)(syst). The measured cross sections are larger than but consistent with the standard model predictions within two standard deviations, and represent the most precise measurement of these cross sections to date.

JOURNAL OF HIGH ENERGY PHYSICS [7], 219, 2023. DOI: 10.1007/JHEP07(2023)219

[P189-2023] "Measurement of the production of charm jets tagged with D-0 mesons in pp collisions at root s=5.02 and 13 TeV"

Acharya, S.; Adamova, D.; **Chinellato, D. D.*; Guardiano, G. G.*; Jahnke, C.*; Takahashi, J.***; et al.
ALICE Collaboration

The measurement of the production of charm jets, identified by the presence of a D-0 meson in the jet constituents, is presented in proton-proton collisions at centre-ofmass energies of root s = 5.02 and 13TeV with the ALICE detector at the CERN LHC. The D-0 mesons were reconstructed from their hadronic decay D-0 -> K- pi(+) and the respective charge conjugate. Jets were reconstructed from D-0-meson candidates and charged particles using the anti- kT algorithm, in the jet transverse momentum range 5 < p(T,chjet) < 50 GeV/c, pseudorapidity |eta(jet)| < 0.9 - R, and with the jet resolution parameters R = 0.2, 0.4, 0.6. The distribution of the jet momentum fraction carried by a D-0 meson along the jet axis (z(broken vertical bar broken vertical bar)(ch)) was measured in the range 0.4 < z(broken vertical bar broken vertical bar)(ch) < 1.0 in four ranges of the jet transverse momentum. Comparisons of results for different collision energies and jet resolution parameters are also presented. The measurements are compared to predictions from Monte Carlo event generators based on leading-order and next-to-leading-order perturbative quantum chromodynamics calculations. A generally good description of the main features of the data is obtained in spite of a few discrepancies at low (pT,chjet). Measurements were also done for R = 0.3 at root s = 5.02 and are shown along with their comparisons to theoretical predictions in an appendix to this paper.

JOURNAL OF HIGH ENERGY PHYSICS [6], 133, 2023. DOI: 10.1007/JHEP06(2023)133

[P190-2023] "Measurements of the groomed jet radius and momentum splitting fraction with the soft drop and dynamical grooming algorithms in pp collisions at root s=5.02 TeV"

Acharya, S.; Adamova, D.; **Chinellato, D. D.*; Guardiano, G. G.*; Jahnke, C.*; Takahashi, J.***; et al.
ALICE Collaboration

This article presents measurements of the groomed jet radius and momentum splitting fraction in pp collisions at root s = 5.02 TeV with the ALICE detector at the Large Hadron Collider. Inclusive charged-particle jets are reconstructed at midrapidity using the anti-k(T) algorithm for transverse momentum 60 < p(T)(ch) (jet) < 80 GeV/c. We report results using two different grooming algorithms: soft drop and, for the first time, dynamical grooming. For each grooming algorithm, a variety of grooming settings are used in order to explore the impact of collinear radiation on these jet substructure observables. These results are compared to perturbative calculations that include resummation of large logarithms at all orders in the strong coupling constant. We find good agreement of the theoretical predictions with the data for all grooming settings considered.

JOURNAL OF HIGH ENERGY PHYSICS [5], 244, 2023. DOI: 10.1007/JHEP05(2023)244

[P191-2023] "Neutrino oscillations in the interaction picture"

Blasone, M.; Giacosa, F.; Smaldone, L.; **Torrieri, G.***

We study the mixing of different kind of fields (scalar in 0+1D, scalar in 3+1D, fermion in 3+1D) treating the mixing term as an interaction. To this aim, we employ the usual perturbative series in the interaction picture. We find that expression for flavor changing probability exhibits corrections with respect to the usual quantum mechanical (e.g. neutrino) oscillation formula, in agreement with the result previously obtained in the non-perturbative flavor Fock space approach.

EUROPEAN PHYSICAL JOURNAL C 83[8], 736, 2023. DOI: 10.1140/epjc/s10052-023-11867-3

[P192-2023] "Neutron emission in ultraperipheral Pb-Pb collisions at sNN=5.02 TeV"

Acharya, S.; Adamova, D.; **Chinellato, D. D.*; Guardiano, G. G.*; Jahnke, C.*; Takahashi, J.***; et al.
ALICE Collaboration

In ultraperipheral collisions (UPCs) of relativistic nuclei without overlap of nuclear densities, the two nuclei are excited by the Lorentz-contracted Coulomb fields of their collision partners. In these UPCs, the typical nuclear excitation energy is below a few tens of MeV, and a small number of nucleons are emitted in electromagnetic dissociation (EMD) of primary nuclei, in contrast to complete nuclear fragmentation in hadronic interactions. The cross sections of emission of given numbers of neutrons in UPCs of 208Pb nuclei at & RADIC;sNN = 5.02 TeV were measured with the neutron zero degree calorimeters (ZDCs) of the ALICE detector at the LHC, exploiting a similar technique to that used in previous studies performed at & RADIC;sNN = 2.76 TeV. In addition, the cross sections for the exclusive emission of one, two, three, four, and five forward neutrons in the EMD, not accompanied by the emission of forward protons, and thus mostly corresponding to the production of 207,206,205,204,203Pb, respectively, were measured for the first time. The predictions from the available models describe the measured cross sections well. These cross sections can be used for evaluating the impact of secondary nuclei on the LHC components, in particular, on superconducting magnets, and also provide useful input for the design of the Future Circular Collider (FCC-hh).

PHYSICAL REVIEW C 107[6], 064902, 2023. DOI: 10.1103/PhysRevC.107.064902

[P193-2023] "Noise assessment of CMOS active pixel sensors for the CYGNO Experiment"

Almeida, B. D.; Amaro, F. D.; **Kemp, E.***; et al.

Active Pixel sensors play a crucial role in enabling successful low-light scientific experiments due to their inherent advantages and capabilities. Such devices not only offer high spatial resolution but also feature individual pixels with integrated amplifiers, allowing for direct signal amplification at the pixel level. This results in reduced readout noise and improved signal-to-noise ratio (SNR), which are particularly vital when dealing with limited photon counts in low-light environments. This holds particularly true for scientific CMOS (sCMOS) sensors, acknowledged as an advanced evolution of Active Pixel sensors. However, despite their advantages, such sensors can still exhibit limitations such as higher cost and presence of noise artifacts that should be closely investigated. In particular, CYGNO project fits in a global effort aimed at direct detection of Dark Matter particles. CYGNO collaboration intends to build a detector based on a Time Projection Chamber making use of Gas Electron Multipliers for the amplification of ionization electrons. The GEM multiplication process produces photons that can be readout by a high-resolution sCMOS sensor.

Such detection system is being designed to have enough sensitivity to detect low-energy particles and to measure released energy with enough granularity so to reconstruct direction and energy profile along their trajectories. The image sensor has an important role in the detector performance, having a direct impact on the SNR of the experiment. This work proposes a study on the performance of three different sCMOS sensors with respect to their sensitivity to low--energy particles and their intrinsic noise, which are of the utmost importance for various scientific experiments.

MEASUREMENT SCIENCE AND TECHNOLOGY 34[12], 125145, 2023. DOI: 10.1088/1361-6501/acf7e1

[P194-2023] "Non-local contribution from small scales in galaxy-galaxy lensing: comparison of mitigation schemes"

Prat, J.; Zacharegkas, G.; **Navarro-Alsina, A.***; et al.
DES Collaboration

Recent cosmological analyses with large-scale structure and weak lensing measurements, usually referred to as 3 x 2pt, had to discard a lot of signal to noise from small scales due to our inability to accurately model non-linearities and baryonic effects. Galaxy-galaxy lensing, or the position-shear correlation between lens and source galaxies, is one of the three two--point correlation functions that are included in such analyses, usually estimated with the mean tangential shear. However, tangential shear measurements at a given angular scale theta or physical scale R carry information from all scales below that, forcing the scale cuts applied in real data to be significantly larger than the scale at which theoretical uncertainties become problematic. Recently, there have been a few independent efforts that aim to mitigate the non-locality of the galaxy-galaxy lensing signal. Here, we perform a comparison of the different methods, including the Y-transformation, the point-mass marginalization methodology, and the annular differential surface density statistic. We do the comparison at the cosmological constraints level in a combined galaxy clustering and galaxy-galaxy lensing analysis. We find that all the estimators yield equivalent cosmological results assuming a simulated Rubin Observatory Legacy Survey of Space and Time (LSST) Year 1 like set-up and also when applied to DES Y3 data. With the LSST Y1 set-up, we find that the mitigation schemes yield similar to 1.3 times more constraining S-8 results than applying larger scale cuts without using any mitigation scheme.

MONTHLY NOTICES OF THE ROYAL ASTRONOMICAL SOCIETY 522[1], 412-425, 2023. DOI: 10.1093/mnras/stad847

[P195-2023] "Observation of magnetic vortex configuration in non-stoichiometric Fe3O4 nanospheres"

Niraula, G.; Toneto, D.; Goya, G. F.; Zoppellaro, G.; Coaquira, J. A. H.; **Muraca, D.*;** Denardin, J. C.; Almeida, T. P.; **Knobel, M.*;** Ayesh, A. I.; Sharma, S. K.

Theoretical and micromagnetic simulation studies of magnetic nanospheres with vortex configurations suggest that such nanostructured materials have technological advantages over conventional nanosystems for applications based on high--power-rate absorption and subsequent emission. However, full experimental evidence of magnetic vortex configurations in spheres of submicrometer size is still lacking. Here, we report the microwave irradiation fabrication of Fe3O4 nanospheres and establish their magnetic vortex configuration based on experimental results, theoretical analysis, and micromagnetic simulations. Detailed magnetic and electrical measurements, together with Mossbauer spectroscopy data, provide evidence of a loss of stoichiometry in vortex nanospheres owing to the presence of a surface oxide layer, defects, and a higher concentration of cation vacancies. The results indicate that the magnetic vortex spin configuration can be established in bulk spherical magnetite materials. This study provides crucial information that can aid the synthesis of magnetic nanospheres with magnetically tailored properties; consequently, they may be promising candidates for future technological applications based on three-dimensional magnetic vortex structures.

NANOSCALE ADVANCES 5[18], 5015-5028, 2023. DOI: 10.1039/d3na00433c

[P196-2023] "Optimizing a two-layer method for hybrid diffuse correlation spectroscopy and frequency-domain diffuse optical spectroscopy cerebral measurements in adults"

Forti, R. M.*; Martins, G. G.*; Baker, W. B.; **Mesquita, R. C.***

Significance: The sensitivity to extracerebral tissues is a well--known confounder of diffuse optics. Two-layer (2L) head models can separate cerebral signals from extracerebral artifacts, but they also carry the risk of crosstalk between fitting parameters.Aim: We aim to implement a constrained 2L head model for hybrid diffuse correlation spectroscopy (DCS) and frequency-domain diffuse optical spectroscopy (FD-DOS) data and to characterize errors in cerebral blood flow and tissue absorption with the proposed model.Approach: The algorithm uses the analytical solution of a 2L cylinder and an a priori extracerebral layer thickness to fit multidistance FD-DOS (0.8 to 4 cm) and DCS (0.8 and 2.5 cm) data, assuming homogeneous tissue reduced scattering. We characterized the algorithm's accuracy for simulated data with noise generated using a 2L slab and realistic adult head geometries and for in vitro phantom data.Results: Our algorithm recovered the cerebral flow index with 6.3 [2.8, 13.2]% and 34 [30, 42]% (median absolute percent error [interquartile range]) for slab and head geometries, respectively. Corresponding errors in the cerebral absorption coefficient were 5.0 [3.0, 7.9]% and 4.6 [2.4, 7.2]% for the slab and head geometries and 8 [5, 12]% for our phantom experiment. Our results were minimally sensitive to second-layer scattering changes and were robust to cross-talk between fitting parameters.Conclusions: In adults, the constrained 2L algorithm promises to improve FD-DOS/DCS accuracy compared with the conventional semi-infinite approach.

NEUROPHOTONICS 10[2], 025008, 2023. DOI: 10.1117/1.NPh.10.2.025008

[P197-2023] "Planar vs Non-Planar Orientation in AuAg-Catalyzed InP Nanowire Growth"

Zavarize, M.*; Sibirev, N. V.; Berdnikov, Y.; **Moreira, M.*; Obata, H. T.*; Rodrigues, V.*; Dubrovskii, V. G.; Cotta, M. A.***

InP nanowires were catalyzed by Au, Ag,and Au x Ag1-x nanoparticleson GaAs substrates with various orientations. Statistical analysisand modeling revealed that the droplet surface density to In precursorflux ratio is crucial in controlling nanowire growth mode and orientation.These findings enhance our understanding of planar nanowire vapor-liquid-solidgrowth and offer tools for controlling III-V nanowire growthon lattice--mismatched substrates. Nanowire integration into currentprocessing technologiesremainsan important challenge regarding scalable device fabrication, particularlyfor metal-catalyzed III--V nanowires integrated with Si-basedelectronics. Controlling nanowire orientation, either in or out ofa substrate plane, by using different metal catalysts may work asa tool to address these issues.Here, we report an extensive investigationof InP nanowires catalyzed by Au, Ag, and Au x Ag1-x nanoparticles grownon GaAs substrates with different orientations. Using statisticalanalysis of the experimental data and modeling,

we show that the ratioof the droplet surface density over the In precursor flux is the keyparameter controlling the nanowire growth mode and spatial orientation. Overall, these results provide further understanding of the vapor-liquid-solidgrowth of planar nanowires and allow us to find tools for the controlof growth orientation of III-V nanowires catalyzed by differentmetallic nanoparticles on lattice-mismatched substrates.

CRYSTAL GROWTH & DESIGN 23[9], 6623-6630, 2023. DOI: 10.1021/acs.cgd.3c00542

[P198-2023] "Production of KS0, Λ ((Λ)over-bar), Ξ±, and Ω± in jets and in the underlying event in pp and p-Pb collisions"

Acharya, S.; Adamova, D.; **Chinellato, D. D.*; Guardiano, G. G.*; Jahnke, C.*; Takahashi, J.***; et al.
ALICE Collaboration

The production of strange hadrons (K-S(0), Lambda, Xi(+/-), and Omega(+/-)), baryon-to-meson ratios (Lambda/K-S(0), Xi/K-S(0), and Omega/K-S(0)), and baryon-to-baryon ratios (Xi/Lambda, Omega/Lambda, and Omega/Xi) associated with jets and the underlying event were measured as a function of transverse momentum (pT) in pp collisions at root s = 13TeV and p-Pb collisions at root s(NN) = 5.02TeV with the ALICE detector at the LHC. The inclusive production of the same particle species and the corresponding ratios are also reported. The production of multi-strange hadrons, Xi(+/-) and Omega(+/-), and their associated particle ratios in jets and in the underlying event are measured for the first time. In both pp and p-Pb collisions, the baryon-to-meson and baryon-to-baryon yield ratios measured in jets differ from the inclusive particle production for low and intermediate hadron p(T) (0.6-6 GeV/ c). Ratios measured in the underlying event are in turn similar to those measured for inclusive particle production. In pp collisions, the particle production in jets is compared with Pythia 8 predictions with three colour-reconnection implementation modes. None of them fully reproduces the data in the measured hadron pT region. The maximum deviation is observed for Xi(+/-) and Omega(+/-) which reaches a factor of about six. The event multiplicity dependence is further investigated in p-Pb collisions. In contrast to what is observed in the underlying event, there is no significant event-multiplicity dependence for particle production in jets. The presented measurements provide novel constraints on hadronisation and its Monte Carlo description. In particular, they demonstrate that the fragmentation of jets alone is insufficient to describe the strange and multi-strange particle production in hadronic collisions at LHC energies.

JOURNAL OF HIGH ENERGY PHYSICS [7], 136, 2023. DOI: 10.1007/JHEP07(2023)136

[P199-2023] "Production of pions, kaons, and protons as a function of the relative transverse activity classifier in pp collisions at root s=13 TeV"

Acharya, S.; Adamova, D.; **Chinellato, D. D.*; Guardiano, G. G.*; Jahnke, C.*; Takahashi, J.***; et al.
ALICE Collaboration

The production of pi (+/-), K-+/-, and ((P) over bar)p is measured in pp collisions at root s = 13TeV in different topological regions of the events. Particle transverse momentum (pT) spectra are measured in the "toward", "transverse", and "away" angular regions defined with respect to the direction of the leading particle in the event. While the toward and away regions contain the fragmentation products of the near-side and away-side jets, respectively, the transverse region is dominated by particles from the Underlying Event (UE). The relative transverse activity classifier, R-T = N-T/< N-T >, is used to group events according to their UE activity, where NT is the measured charged-particle multiplicity per event in the transverse region and < N-T > is the mean value over all the analysed events. The first measurements of identified particle p(T) spectra as a function of R-T in the three topological regions are reported. It is found that the yield of high transverse momentum particles relative to the R-T-integrated measurement decreases with increasing R-T in both the toward and the away regions, indicating that the softer UE dominates particle production as RT increases and validating that R-T can be used to control the magnitude of the UE. Conversely, the spectral shapes in the transverse region harden significantly with increasing RT. This hardening follows a mass ordering, being more significant for heavier particles. Finally, it is observed that the pT-differential particle ratios (p + (P) over bar)/(pi(+) + pi(-)) and (K+ + K-)/(pi(+) + K-) in the low UE limit (R-T -> 0) approach expectations from Monte Carlo generators such as PYTHIA 8 with Monash 2013 tune and EPOS LHC, where the jet-fragmentation models have been tuned to reproduce e(+)e(-) results.

JOURNAL OF HIGH ENERGY PHYSICS [6], 27, 2023. DOI: 10.1007/JHEP06(2023)027

[P200-2023] "Search for a heavy composite Majorana neutrino in events with dilepton signatures from proton-proton collisions at root s=13 Tev"

Tumasyan, A.; Adam, W.; **Chinellato, J. A.***; et al.
CMS Collaboration

Results are presented of a search for a heavy Majorana neutrino N : decaying into two same-flavor leptons : (electrons or muons) and a quark-pair jet. A model is considered in which the N : is an excited neutrino in a compositeness scenario. The analysis is performed using a sample of proton-proton collisions at & RADIC;s = 13 TeV recorded by the CMS experiment at the CERN LHC, corresponding to an integrated luminosity of 138 fb-1. The data are found to be in agreement with the standard model prediction. For the process in which the N : is produced in association with a lepton, followed by the decay of the N : to a same-flavor lepton and a quark pair, an upper limit at 95% confidence level on the product of the cross section and branching fraction is obtained as a function of the N : mass mN : and the compositeness scale :. For this model the data exclude the existence of Ne (N & mu;) for mN : below 6.0 (6.1) TeV, at the limit where mN : is equal to :. For mN : N 1 TeV, values of : less than 20 (23) TeV are excluded. These results represent a considerable improvement in sensitivity, covering a larger parameter space than previous searches in pp collisions at 13 TeV.& COPY; 2023 The Author(s). Published by Elsevier B.V. This is an open access article under the CC BY license (http://creativecommons .org /licenses /by /4 .0/). Funded by SCOAP3.

PHYSICS LETTERS B 843, 137803, 2023. DOI: 10.1016/j.physletb.2023.137803

[P201-2023] "Search for a massive scalar resonance decaying to a light scalar and a Higgs boson in the four b quarks final state with boosted topology"

Tumasyan, A. ;Adam, W.; **Chinellato, J. A.***; et al.
CMS Collaboration

We search for new massive scalar particles X and Y through the resonant process X & RARR; YH & RARR; bb bb, where H is the standard model Higgs boson. Data from CERN LHC proton--proton collisions are used, collected at a centre-of-mass energy of 13 TeV in 2016-2018 and corresponding to an integrated luminosity of 138 fb-1. The search is performed in mass ranges of 0.9-4 TeV for X and 60-600 GeV for Y, where both Y and H are reconstructed as Lorentz-boosted single large-area jets.

The results are interpreted in the context of the next-to--minimal supersymmetric standard model and also in an extension of the standard model with two additional singlet scalar fields. The 95% confidence level upper limits for the production cross section vary between 0.1 and 150 fb depending on the X and Y masses, and represent a significant improvement over results from previous searches.& COPY; 2022 The Author(s). Published by Elsevier B.V. This is an open access article under the CC BY license (http://creativecommons .org /licenses /by /4 .0/). Funded by SCOAP3.

PHYSICS LETTERS B 842, 137392, 2023. DOI: 10.1016/j.physletb.2022.137392

[P202-2023] "Search for CP violation using t (t)over-bar events in the lepton plus jets channel in pp collisions at root s=13 TeV"

Tumasyan, A.; Adam, W.; **Chinellato, J. A.***; et al.
CMS Collaboration

Results are presented on a search for CP violation in the production and decay of top quark-antiquark pairs in the lepton+jets channel. The search is based on data from proton--proton collisions at root s = 13TeV, collected with the CMS detector, corresponding to an integrated luminosity of 138 fb(-1). Possible CP violation effects are evaluated by measuring asymmetries in observables constructed from linearly independent four-momentum vectors of the final-state particles. The dimensionless chromoelectric dipole moment of the top quark obtained from the observed asymmetries is measured to be 0.04 +/- 0.10 (stat)+/- 0.07(syst), and the asymmetries exhibit no evidence for CP-violating effects, consistent with expectations from the standard model.

JOURNAL OF HIGH ENERGY PHYSICS [6], 81, 2023. DOI: 10.1007/JHEP06(2023)081

[P203-2023] "Search for heavy resonances and quantum black holes in e mu, e tau, and mu tau final states in proton--proton collisions at root s=13 TeV"

Tumasyan, A. ;Adam, W.; **Chinellato, J. A.***; et al.
CMS Collaboration

A search is reported for heavy resonances and quantum black holes decaying into e mu, e tau, and mu tau final states in proton-proton collision data recorded by the CMS experiment at the CERN LHC during 2016-2018 at root s = 13TeV, corresponding to an integrated luminosity of 138 fb(-1). The e mu, e tau, and mu tau invariant mass spectra are reconstructed, and no evidence is found for physics beyond the standard model. Upper limits are set at 95% confidence level on the product of the cross section and branching fraction for lepton flavor violating signals. Three benchmark signals are studied: resonant tau sneutrino production in R parity violating supersymmetric models, heavy Z' gauge bosons with lepton flavor violating decays, and nonresonant quantum black hole production in models with extra spatial dimensions. Resonant tau sneutrinos are excluded for masses up to 4.2TeV in the e mu channel, 3.7TeV in the e tau channel, and 3.6TeV in the mu tau channel. A Z' boson with lepton flavor violating couplings is excluded up to a mass of 5.0TeV in the e mu channel, up to 4.3Te V in the e tau channel, and up to 4.1TeV in the mu tau channel. Quantum black holes in the benchmark model are excluded up to the threshold mass of 5.6TeV in the e mu channel, 5.2Te V in the e tau channel, and 5.0TeV in the mu tau channel. In addition, model-independent limits are extracted to allow comparisons with other models for the same final states and similar event selection requirements. The results of these searches provide the most stringent limits available from collider experiments for heavy particles that undergo lepton flavor violating decays.

JOURNAL OF HIGH ENERGY PHYSICS [5], 227, 2023. DOI: 10.1007/JHEP05(2023)227

[P204-2023] "Search for Higgs boson decays into Z and J/psi and for Higgs and Z boson decays into J/psi or Y pairs in pp collisions at root s=13 TeV"

Tumasyan, A.; Adam, W.; **Chinellato, J. A.*;** et al.
CMS Collaboration

Decays of the Higgs boson into a Z boson and a J/& psi; or & psi;(2S) meson are searched for in four-lepton final states with the CMS detector at the LHC. A data set of proton-proton collisions corresponding to an integrated luminosity of 138 fb-1 is used. Using the same data set, decays of the Higgs and Z boson into quarkonium pairs are also searched for. An observation of such decays with this sample would indicate the presence of physics beyond the standard model. No evidence for these decays has been observed and upper limits at the 95% confidence level are placed on the corresponding branching fractions (B). Assuming longitudinal polarization of the Higgs boson decay products, 95% confidence level observed upper limits for B(H & RARR; ZJ/& psi;) and B(H & RARR; Z & psi;(2S)) are 1.9 x 10-3 and 6.6 x 10-3, respectively.& COPY; 2022 The Author(s). Published by Elsevier B.V. This is an open access article under the CC BY license (http://creativecommons .org /licenses /by /4 .0/). Funded by SCOAP3.

PHYSICS LETTERS B 842, 137534, 2023. DOI: 10.1016/j.physletb.2022.137534

[P205-2023] "Search for Higgs boson decays to a Z boson and a photon in proton-proton collisions at root s=13 TeV"

Tumasyan, A. ;Adam, W.; **Chinellato, J. A.***; et al.
CMS Collaboration

Results are presented from a search for the Higgs boson decay H -> Z gamma, where Z -> l(+) l(-) with l = e or mu. The search is performed using a sample of proton-proton (pp) collision data at a center-of-mass energy of 13TeV, recorded by the CMS experiment at the LHC, corresponding to an integrated luminosity of 138 fb(-1). Events are assigned to mutually exclusive categories, which exploit differences in both event topology and kinematics of distinct Higgs production mechanisms to enhance signal sensitivity. The signal strength mu, defined as the product of the cross section and the branching fraction [sigma(pp -> H) B (H -> Z gamma)] relative to the standard model prediction, is extracted from a simultaneous fit to the l(+) l(-) gamma invariant mass distributions in all categories and is measured to be mu = 2.4 +/- 0.9 for a Higgs boson mass of 125.38 GeV. The statistical significance of the observed excess of events is 2.7 standard deviations. This measurement corresponds to sigma (pp -> H) B(H -> Z gamma) = 0.21 +/- 0.08 pb. The observed (expected) upper limit at 95% confidence level on mu is 4.1 (1.8), where the expected limit is calculated under the background-only hypothesis. The ratio of branching fractions B(H -> Z gamma)/ B(H -> gamma gamma) is measured to be 1.5(-0.6)(+0.7), which agrees with the standard model prediction of 0.69 +/- 0.04 at the 1.5 standard deviation level.

JOURNAL OF HIGH ENERGY PHYSICS [5], 233, 2023. DOI: 10.1007/JHEP05(2023)233

[P206-2023] "Search for long-lived particles decaying to a pair of muons in proton-proton collisions at root s=13 TeV"

Tumasyan, A.; Adam, W.; **Chinellato, J. A.***; et al.
CMS Collaboration

An inclusive search for long-lived exotic particles decaying to a pair of muons is presented. The search uses data collected by the CMS experiment at the CERN LHC in proton-proton collisions at root s = 13 TeV in 2016 and 2018 and corresponding to an integrated luminosity of 97.6 fb(-1). The experimental signature is a pair of oppositely charged muons originating from a common secondary vertex spatially separated from the pp interaction point by distances ranging from several hundred mu m to several meters. The results are interpreted in the frameworks of the hidden Abelian Higgs model, in which the Higgs boson decays to a pair of long-lived dark photons Z(D), and of a simplified model, in which long-lived particles are produced in decays of an exotic heavy neutral scalar boson. For the hidden Abelian Higgs model with m(Z(D)) greater than 20 GeV and less than half the mass of the Higgs boson, they provide the best limits to date on the branching fraction of the Higgs boson to dark photons for c tau(Z(D)) (varying with m(Z(D))) between 0.03 and approximate to 0.5 mm, and above approximate to 0.5 m. Our results also yield the best constraints on long-lived particles with masses larger than 10 GeV produced in decays of an exotic scalar boson heavier than the Higgs boson and decaying to a pair of muons.

JOURNAL OF HIGH ENERGY PHYSICS [5], 228, 2023. DOI: 10.1007/JHEP05(2023)228

[P207-2023] "Search for long-lived particles using out-of--time trackless jets in proton-proton collisions at √s=13 TeV"

Tumasyan, A.; Adam, W.; **Chinellato, J. A.***; et al.
CMS Collaboration

A search for long-lived particles decaying in the outer regions of the CMS silicon tracker or in the calorimeters is presented. The search is based on a data sample of proton-proton collisions at root s = 13TeV recorded with the CMS detector at the LHC in 2016-2018, corresponding to an integrated luminosity of 138 fb(-1). A novel technique, using nearly trackless and out-of-time jet information combined in a deep neural network discriminator, is employed to identify decays of long-lived particles. The results are interpreted in a simplified model of chargino-neutralino production, where the neutralino is the next-to-lightest supersymmetric particle, is long-lived, and decays to a gravitino and either a Higgs or Z boson. This search is most sensitive to neutralino proper decay lengths of approximately 0.5 m, for which masses up to 1.18TeV are excluded at 95% confidence level. The current search is the best result to date in the mass range from the kinematic limit imposed by the Higgs boson mass up to 1.8TeV.

JOURNAL OF HIGH ENERGY PHYSICS 7, 210, 2023. DOI: 10.1007/JHEP07(2023)210

[P208-2023] "Search for nonresonant Higgs boson pair production in final state with two bottom quarks and two tau leptons in proton-proton collisions at s=13 TeV"

Tumasyan, A.; Adam, W.; **Chinellato, J. A.***; et al.
CMS Collaboration

A search for the nonresonant production of Higgs boson pairs (HH) via gluon-gluon and vector boson fusion processes in final states with two bottom quarks and two tau leptons is presented. The search uses data from proton-proton collisions at a center-of-mass energy of & RADIC;s = 13 TeV recorded with the CMS detector at the LHC, corresponding to an integrated luminosity of 138 fb-1. Events in which at least one tau lepton decays hadronically are considered and multiple machine learning techniques are used to identify and extract the signal. The data are found to be consistent, within uncertainties, with the standard model (SM) predictions. Upper limits on the HH production cross section are set to constrain the parameter space for anomalous Higgs boson couplings. The observed (expected) upper limit at 95% confidence level corresponds to 3.3 (5.2) times the SM prediction for the inclusive HH cross section and to 124 (154) times the SM prediction for the vector boson fusion HH cross section. At 95% confidence level, the Higgs field self-coupling is constrained to be within -1.7 and 8.7 times the SM expectation, and the coupling of two Higgs bosons to two vector bosons is constrained to be within -0.4 and 2.6 times the SM expectation. & COPY; 2022 The Author(s). Published by Elsevier B.V. This is an open access article under the CC BY license (http://creativecommons .org /licenses /by /4 .0/). Funded by SCOAP3.

PHYSICS LETTERS B 842, 137531, 2023. DOI: 10.1016/j.physletb.2022.137531

[P209-2023] "Search for nonresonant Higgs boson pair production in the four leptons plus twob jets final state in proton-proton collisions at root s=13 TeV"

Tumasyan, A.; Adam, W.; **Chinellato, J. A.***; et al.
CMS Collaboration

The first search for nonresonant production of Higgs boson pairs (HH) with one H decaying into four leptons and the other into a pair of b quarks is presented, using proton-proton collisions recorded at a center-of-mass energy of root s = 13TeV by the CMS experiment. The analyzed data correspond to an integrated luminosity of 138 fb(-1). A 95% confidence level upper limit of 32.4 is set on the signal strength modifier mu, defined as the ratio of the observed HH production rate in the HH -> ZZ* b (b) over bar -> 4 lb (b) over bar decay channel to the standard model (SM) expectation. Possible modifications of the H trilinear coupling lambda(HHH) with respect to the SM value are investigated. The coupling modifier kappa(lambda), defined as lambda(HHH) divided by its SM prediction, is constrained to be within the observed (expected) range -8.8 (-9.8) < kappa(lambda) < 13.4 (15.0) at 95% confidence level.

JOURNAL OF HIGH ENERGY PHYSICS [6], 130, 2023. DOI: 10.1007/JHEP06(2023)130

[P210-2023] "Search for photons above 1019 eV with the surface detector of the Pierre Auger Observatory"

Abreu, P.; Aglietta, M.; **Arbeletche, L. B.*; Chinellato, J. A.*; Franco, D. de O.*; Dobrigkeit, C.*; Fauth, A. C.*; Payeras, A. M.***; et al.
Pierre Auger Collaboration

We use the surface detector of the Pierre Auger Observatory to search for air showers initiated by photons with an energy above 1019 eV. Photons in the zenith angle range from 30 & DEG; to 60 & DEG; can be identified in the overwhelming background of showers initiated by charged cosmic rays through the broader time structure of the signals induced in the water Cherenkov detectors of the array and the steeper lateral distribution of shower particles reaching ground. Applying the search method to data collected between January 2004 and June 2020, upper limits at 95% CL are set to an E-2 diffuse flux of ultra-high energy photons above 1019 eV, 2x1019 eV and 4x1019 eV amounting to 2.11x10-3, 3.12x10-4 and 1.72x10-4 km-2 sr-1 yr-1, respectively. While the sensitivity of the present search around 2 x 1019 eV approaches expectations of cosmogenic photon fluxes in the case of a pure-proton composition, it is one order of magnitude above those from more realistic mixed-composition models. The inferred limits have also implications for the search of super-heavy dark matter that are discussed and illustrated.

JOURNAL OF COSMOLOGY AND ASTROPARTICLE PHYSICS [5], 021, 2023. DOI: 10.1088/1475-7516/2023/05/021

[P211-2023] "Search for resonant and nonresonant production of pairs of dijet resonances in proton-proton collisions at √s=13 TeV"

Tumasyan, A.; Adam, W.; **Chinellato, J. A.***; et al.
CMS Collaboration

A search for pairs of dijet resonances with the same mass is conducted in final states with at least four jets. Results are presented separately for the case where the four jet production proceeds via an intermediate resonant state and for nonresonant production. The search uses a data sample corresponding to an integrated luminosity of 138 fb(-1) collected by the CMS detector in proton-proton collisions at root s = 13 TeV. Model-independent limits, at 95% confidence level, are reported on the production cross section of four-jet and dijet resonances. These first LHC limits on resonant pair production of dijet resonances via high mass intermediate states are applied to a signal model of diquarks that decay into pairs of vector-like quarks, excluding diquark masses below 7.6 TeV for a particular model scenario. There are two events in the tails of the distributions, each with a four-jet mass of 8 TeV and an average dijet mass of 2 TeV, resulting in local and global significances of 3.9 and 1.6 standard deviations, respectively, if interpreted as a signal. The nonresonant search excludes pair production of top squarks with masses between 0.50 TeV to 0.77 TeV, with the exception of a small interval between 0.52 and 0.58 TeV, for supersymmetric R-parity-violating decays to quark pairs, significantly extending previous limits. Here, the most significant excess above the predicted background occurs at an average dijet mass of 0.95 TeV, for which the local and global significances are 3.6 and 2.5 standard deviations, respectively.

JOURNAL OF HIGH ENERGY PHYSICS [7], 161, 2023. DOI: 10.1007/JHEP07(2023)161

[P212-2023] "Search for top squarks in the four-body decay mode with single lepton final states in proton-proton collisions at root s=13 TeV"

Tumasyan, A.; Adam, W.; **Chinellato, J. A.***; et al.
CMS Collaboration

A search for the pair production of the lightest supersymmetric partner of the top quark, the top squark ((t) over tilde (1)), is presented. The search targets the four-body decay of the (t) over tilde (1), which is preferred when the mass difference between the top squark and the lightest supersymmetric particle is smaller than the mass of the W boson. This decay mode consists of a bottom quark, two other fermions, and the lightest neutralino ((x) over tilde (0)(1)), which is assumed to be the lightest supersymmetric particle. The data correspond to an integrated luminosity of 138 fb(-1) of proton-proton collisions at a center-of-mass energy of 13TeV collected by the CMS experiment at the CERN LHC. Events are selected using the presence of a high-momentum jet, an electron or muon with low transverse momentum, and a significant missing transverse momentum. The signal is selected based on a multivariate approach that is optimized for the difference between m((t) over tilde (1)) and m((x) over tilde (0)(1)). The contribution from leading background processes is estimated from data. No significant excess is observed above the expectation from standard model processes. The results of this search exclude top squarks at 95% confidence level for masses up to 480 and 700 GeV for m((t) over tilde (1))- m((x) over tilde (0)(1)) = 10 and 80 GeV, respectively.

JOURNAL OF HIGH ENERGY PHYSICS [6], 60, 2023. DOI: 10.1007/JHEP06(2023)060

[P213-2023] "Search for Ultra-high-energy Photons from Gravitational Wave Sources with the Pierre Auger Observatory"

Halim, A. A.; Abreu, P.; **Bonneau Arbeletche, L.*; Chinellato, J. A.*; Franco, D. de O.*; Dobrigkeit, C.*; Fauth, A. C.*; Machado Payeras, A.***; et al.
Pierre Auger Collaboration

A search for time-directional coincidences of ultra-high-energy (UHE) photons above 10 EeV with gravitational wave (GW) events from the LIGO/Virgo runs O1 to O3 is conducted with the Pierre Auger Observatory. Due to the distinctive properties of photon interactions and to the background expected from hadronic showers, a subset of the most interesting GW events is selected based on their localization quality and distance. Time periods of 1000 s around and 1 day after the GW events are analyzed. No coincidences are observed. Upper limits on the UHE photon fluence from a GW event are derived that are typically at & SIM;7 MeV cm(-2) (time period 1000 s) and & SIM;35 MeV cm(-2) (time period 1 day). Due to the proximity of the binary neutron star merger GW170817, the energy of the source transferred into UHE photons above 40 EeV is constrained to be less than 20% of its total GW energy. These are the first limits on UHE photons from GW sources.

ASTROPHYSICAL JOURNAL 952[1], 91, 2023. DOI: 10.3847/1538-4357/acc862

[P214-2023] "Searches for additional Higgs bosons and for vector leptoquarks in ττ final states in proton-proton collisions at √s=13 TeV"

Tumasyan, A.; Adam, W.; **Chinellato, J. A.***; et al.
CMS Collaboration

Three searches are presented for signatures of physics beyond the standard model (SM) in tau tau final states in proton--proton collisions at the LHC, using a data sample collected with the CMS detector at root s = 13 TeV, corresponding to an integrated luminosity of 138 fb(-1). Upper limits at 95% confidence level (CL) are set on the products of the branching fraction for the decay into tau leptons and the cross sections for the production of a new boson phi, in addition to the H(125) boson, via gluon fusion (gg phi) or in association with b quarks, ranging from O(10 pb) for a mass of 60 GeV to 0.3 fb for a mass of 3.5TeV each. The data reveal two excesses for gg phi production with local p-values equivalent to about three standard deviations at m(phi) = 0.1 and 1.2TeV. In a search for t-channel exchange of a vector leptoquark U-1, 95% CL upper limits are set on the dimensionless U1 leptoquark coupling to quarks and tau leptons ranging from 1 for a mass of 1TeV to 6 for a mass of 5TeV, depending on the scenario. In the interpretations of the M-h(125) and M-h,EFT(125) minimal supersymmetric SM benchmark scenarios, additional Higgs bosons with masses below 350 GeV are excluded at 95% CL.

JOURNAL OF HIGH ENERGY PHYSICS [7], 73, 2023. DOI: 10.1007/JHEP07(2023)073

[P215-2023] "Sigma(1385)(+/-) resonance production in Pb--Pb collisions at root sNN=5.02 TeV"

Acharya, S.; Adamova, D.; **Chinellato, D. D.*; Guardiano, G. G.*; Jahnke, C.*; Takahashi, J.***; et al.
ALICE Collaboration

Hadronic resonances are used to probe the hadron gas produced in the late stage of heavy-ion collisions since they decay on the same timescale, of the order of 1-10 fm/c, as the decoupling time of the system. In the hadron gas, (pseudo)elastic scatterings among the products of resonances that decayed before the kinetic freeze-out and regeneration processes counteract each other, the net effect depending on the resonance lifetime, the duration of the hadronic phase, and the hadronic cross sections at play.

In this context, the Sigma(1385)(+/-) particle is of particular interest as models predict that regeneration dominates over rescattering despite its relatively short lifetime of about 5.5 fm/c. The first measurement of the Sigma(1385)(+/-) resonance production at midrapidity in Pb-Pb collisions at root sNN = 5.02 TeV with the ALICE detector is presented in this Letter. The resonances are reconstructed via their hadronic decay channel, Lambda pi, as a function of the transverse momentum (pT) and the collision centrality. The results are discussed in comparison with the measured yield of pions and with expectations from the statistical hadronization model as well as commonly employed event generators, including PYTHIA8/Angantyr and EPOS3 coupled to the UrQMD hadronic cascade afterburner. None of the models can describe the data. For Sigma(1385)(+/-), a similar behaviour as K*(892)(0) is observed in data unlike the predictions of EPOS3 with afterburner.

EUROPEAN PHYSICAL JOURNAL C 83[5], 351, 2023. DOI: 10.1140/epjc/s10052-023-11475-1

[P216-2023] "Solar-based photocatalytic ozonation employing novel S-scheme ZnO/Cu2O/CuO/carbon xerogel photocatalyst: effect of pH, salinity, turbidity, and temperature on salicylic acid degradation"

Moraes, N. P. de; Santos, R. D. M. dos; Gouvea, M. E. V.; **Siervo, A. de***; Rocha, R. D. da S.; Reddy, D. A.; Yu, L. Q.; Lanza, M. R. de V.; Rodrigues, L. A.

This paper proposes the study of a solar-based photocatalytic ozonation process for the degradation of salicylic acid (SA) using a novel S-scheme ZnO/Cu2O/CuO/carbon xerogel photocatalyst. The incorporation of CuO and Cu2O aims to enhance charge mobility through the formation of p-n heterojunctions with ZnO, whereas the carbon xerogel (XC) was selected due to its eco-friendly nature, capacity to stabilize S-scheme heterojunctions as a solid-state electron mediator, and ability to function as a reducing agent under high temperatures. The characterization of the composites demonstrates that the presence of the XC during the calcination step led to the reduction of a fraction of the CuO into Cu2O, forming a ternary semiconductor heterojunction system. In terms of photocatalysis, the XC/ZnO-CuxO 5% composite achieved the best efficiency for salicylic acid degradation, mainly due to the stabilization of the S-scheme charge transfer pathway between the ZnO/CuO/Cu2O semiconductors by the XC. The total organic carbon (TOC) removal during heterogeneous photocatalysis was 80% for the solar-based process and 68% for the visible light process, after 300 min. The solar-based photocatalytic ozonation process was highly successful regarding the degradation of SA, achieving a 75% increase in the apparent reaction rate constant when compared to heterogeneous photocatalysis. Furthermore, a 78% TOC removal was achieved after 150 min, which is half the time required by the heterogeneous photocatalysis to obtain the same result. Temperature, salinity, and turbidity had major effects on the efficiency of the photocatalytic ozonation process; the system's pH did not cause any major performance variation, which holds relevance for industrial applications.

ENVIRONMENTAL SCIENCE AND POLLUTION RESEARCH 30[43], 98211-98230, 2023. DOI: 10.1007/s11356-023-29399-4

[P217-2023] "Stable Surface-Plasmon Resonances in Small Alumina-Embedded Silver Clusters"

Moreira, M. H.*; Cottancin, E.; Pellarin, M.; Boisron, O.; **Rodrigues, V***.; Lerme, J.; **Hillenkamp, M.***

Localized surface-plasmon resonances are ubiquitous for the characterization and in applications of noble metal nanoparticles. Their dependence on the chemical composition, size, shape, and environment has been widely studied for decades, but still many aspects are the subject of controversy. In this article, we experimentally investigate surfactant-free and mass-selected silver nanoparticles embedded in alumina matrices in the size range between several atoms and more than 4 nm diameter, spanning the whole range from large nanoparticles, accurately described by classical Mie theory, down into the range of quantum size effects. Strong and stable resonances are observed for all sizes down to less than 50 atoms, i.e., similar to 1 nm diameter, without significant line shift or broadening as a function of size. With the help of semiquantal simulations, we identify all signals as surface-plasmon resonances. The absence of peak shifts is rationalized as being due to the dielectric oxide environment and the constant width of the resonances as a convolution of inhomogeneities in the local environment and inherent broadening due to Landau damping. We discuss our results in comparison with ligand-stabilized nanoclusters and rationalize the different contributions to the Hamiltonian describing the systems.

JOURNAL OF PHYSICAL CHEMISTRY C 127[36], 17828-17835, 2023. DOI: 10.1021/acs.jpcc.3c03200

[P218-2023] "Strange hadron collectivity in pPb and PbPb collisions"

Tumasyan, A.; Adam, W.; **Chinellato, J. A.***; et al.
CMS Collaboration

The collective behavior of K-S(0) and Lambda/(Lambda) over bar strange hadrons is studied by measuring the elliptic azimuthal anisotropy (v(2)) using the scalar-product and multiparticle correlation methods. Proton-lead (pPb) collisions at a nucleon-nucleon center-of-mass energy root s(NN) = 8.16 TeV and lead-lead (PbPb) collisions at root s(NN) = 5.02 TeV collected by the CMS experiment at the LHC are investigated. Nonflow effects in the pPb collisions are studied by using a subevent cumulant analysis and by excluding events where a jet with transverse momentum greater than 20 GeV is present. The strange hadron v(2) values extracted in pPb collisions via the four- and six-particle correlation method are found to be nearly identical, suggesting the collective behavior. Comparisons of the pPb and PbPb results for both strange hadrons and charged particles illustrate how event-by-event flow fluctuations depend on the system size.

JOURNAL OF HIGH ENERGY PHYSICS [5], 007, 2023. DOI: 10.1007/JHEP05(2023)007

[P219-2023] "Structure-directing ability of the kraft-lignin/cellulose carbon xerogel for the development of C-Nb2O5 sunlight-active photocatalysts"

Moraes, N. P. de; **Siervo, A. de***; Campos, T. M.; Thim, G. P.; Rodrigues, L. A.

This work explored the development of C-Nb2O5 materials through the use of kraft lignin/cellulose carbon xerogel as a structure-directing agent in a simple precipitation synthesis pathway. This strategy was based on xerogel's low-cost and environmentally friendly nature, as well as the lignin's ability to promote structural changes through the chelation of metallic ions and stabilization of crystalline phases. The results showed that the addition of higher quantities of the kraft lignin/cellulose xerogel during the synthesis resulted in the formation of the hexagonal crystalline structure of niobium oxide, whereas the synthesis without the carbonaceous phase led to hexagonal K3NbO2F4 structure. The presence of the carbon xerogel also led to significant morphological changes, such as the formation of rod-like particles with smaller sizes and the augmentation of the specific surface area and pore volume. EDS and XPS show that the hexagonal Nb2O5 obtained was also doped with K and F atoms.

The addition of the carbonaceous phase also led to the reduction of the bandgap energy of materials, whereas an increase in the calcination temperature caused a similar bandgap reduction. The material with the highest carbon content (Nb--0.25L) achieved the highest photoresponse under simulated solar light for the simultaneous photodegradation of methylene blue (MB) and photoreduction of Cr (VI), probably due to its lower bandgap energy, higher surface area, and enhanced methylene blue adsorption capacity. The effect of the calcination temperature implied that dye sensitization was an important factor for the Cr (VI) photoreduction, as faster MB degradation rates led to the suppression of Cr (VI) reduction. Finally, the study of the pH effect on the process showed that higher MB adsorption capacities are linked to higher MB removal rates, which coupled with mechanistic evaluation, proves that MB photodegradation is mainly linked to the direct oxidation reaction promoted by photogenerated vacancies.

JOURNAL OF PHOTOCHEMISTRY AND PHOTOBIOLOGY A--CHEMISTRY 441, 114697, 2023. DOI: 10.1016/j.jphotochem.2023.114697

[P220-2023] "Symmetry plane correlations in Pb-Pb collisions at √sNN=2.76 TeV"

Acharya, S.; Adamova, D.; **Chinellato, D. D.*; Guardiano, G. G.*; Jahnke, C.*; Takahashi, J.***; et al.
ALICE Collaboration

A newly developed observable for correlations between symmetry planes, which characterize the direction of the anisotropic emission of produced particles, is measured in Pb-Pb collisions at root s(NN) = 2.76 TeV with ALICE. This so-called Gaussian Estimator allows for the first time the study of these quantities without the influence of correlations between different flow amplitudes. The centrality dependence of various correlations between two, three and four symmetry planes is presented. The ordering of magnitude between these symmetry plane correlations is discussed and the results of the Gaussian Estimator are compared with measurements of previously used estimators. The results utilizing the new estimator lead to significantly smaller correlations than reported by studies using the Scalar Product method. Furthermore, the obtained symmetry plane correlations are compared to state-of-the-art hydrodynamic model calculations for the evolution of heavy--ion collisions. While the model predictions provide a qualitative description of the data, quantitative agreement is not always observed, particularly for correlators with significant non-linear response of the medium to initial state anisotropies of the collision system. As these results provide unique and independent information, their usage in future Bayesian analysis can further constrain our knowledge on the properties of the QCDmatter produced in ultrarelativistic heavy-ion collisions.

EUROPEAN PHYSICAL JOURNAL C 83[7], 576, 2023. DOI: 10.1140/epjc/s10052-023-11658-w

[P221-2023] "The Dark Energy Survey Year 3 and eBOSS: constraining galaxy intrinsic alignments across luminosity and colour space"

Samuroff, S.; Mandelbaum, R.; **Navarro-Alsina, A.***; et al.
DES Collaboration

We present direct constraints on galaxy intrinsic alignments (IAs) using the Dark Energy Survey Year 3 (DES Y3), the Extended Baryon Oscillation Spectroscopic Survey (eBOSS), and its precursor, the Baryon Oscillation Spectroscopic Survey (BOSS). Our measurements incorporate photometric red sequence (redMaGiC) galaxies from DES with median redshift z similar to 0.2-1.0, luminous red galaxies from eBOSS at z similar to 0.8, and also an SDSS-III BOSS CMASS sample at z similar to 0.5. We measure two-point IA correlations, which we fit using a model that includes lensing, magnification, and photometric redshift error. Fitting on scales 6 Mpc h(-1) < r(p) < 70 Mpc h(-1) , we make a detection of IAs in each sample, at 5 sigma-22 sigma (assuming a simple one-parameter model for IAs). Using these red samples, we measure the IA-luminosity relation. Our results are statistically consistent with previous results, but offer a significant improvement in constraining power, particularly at low luminosity. With this impro v ed precision, we see detectable dependence on colour between broadly defined red samples. It is likely that a more sophisticated approach than a binary red/blue split, which jointly considers colour and luminosity dependence in the IA signal, will be needed in future. We also compare the various signal components at the best-fitting point in parameter space for each sample, and find that magnification and lensing contribute similar to 2 -18 per cent of the total signal. As precision continues to improve, it will certainly be necessary to account for these effects in future direct IA measurements. Finally, we make equivalent measurements on a sample of emission--line galaxies from eBOSS at z similar to 0.8. We constrain the non-linear alignment amplitude to be A(1) = 0.07(-0.42) (+0.32) (vertical bar A(1)vertical bar < 0.78 at 95 per cent CL).

MONTHLY NOTICES OF THE ROYAL ASTRONOMICAL SOCIETY 524[2], 2195-2223, 2023. DOI: 10.1093/mnras/stad2013

[P222-2023] "Thirty Years of Functional Near-Infrared Spectroscopy"

Highton, D.; Boas, D.; Minagawa, Y.; **Mesquita, R. C.***; Gervain, J.

Functional Near-Infrared Spectroscopy (fNIRS) is a non-invasive optical technique that measures cerebral hemodynamics across multiple regions of interest, and thereby characterises brain functional activation. Since its first description in 1993, fNIRS has undergone substantial developments in hardware, analysis techniques, and applications. Thirty years later, this technique is significantly enchancing our understanding in diverse areas of neuroscience research such as neurodevelopment, cognitive neuroscience, psychiatric disorders, neurodegenerative conditions, and brain injury management in intensive care settings. This special issue outlines the latest progress in instrumentation and analysis techniques and showcases some applications within the expanding field of fNIRS over the past decade.

NEUROPHOTONICS 10[2], 023501, 2023. DOI: 10.1117/1.NPh.10.2.023501

[P223-2023] "Topological Hall effect in CeAlGe"

Piva, M. M.; **Souza, J. C.*; Lombardi, G. A.*; Pakuszewski, K. R.*; Adriano, C.*; Pagliuso, P. G.***; Nicklas, M.

The Weyl semimetal CeAlGe is a promising material to study nontrivial topologies in real and momentum space due to the presence of a topological magnetic phase. Our results at ambient pressure show that the electronic properties of CeAlGe are extremely sensitive to small stoichiometric variations. In particular, the topological Hall effect (THE) present in CeAlGe is absent in some samples of almost identical chemical composition. The application of external pressure favors the antiferromagnetic ground state. It also induces a THE where it was not visible at ambient pressure. Furthermore, a small pressure is sufficient to drive the single region of the THE in magnetic fields into two different ones. Our results reveal an extreme sensitivity of the electronic properties of CeAlGe to tiny changes in its chemical composition, leading to a high tunability by external stimuli. We can relate this sensitivity to a shift in the Fermi level and to domain walls.

PHYSICAL REVIEW MATERIALS 7[7], 074204, 2023. DOI: 10.1103/PhysRevMaterials.7.074204

[P224-2023] "Towards the understanding of the genuine three-body interaction for p-p-p and p-p-Lambda"

Acharya, S.; Adamova, D.; **Chinellato, D. D.*; Guardiano, G. G.*; Jahnke, C.*; Takahashi, J.***; et al.
ALICE Collaboration

Three-body nuclear forces play an important role in the structure of nuclei and hypernuclei and are also incorporated in models to describe the dynamics of dense baryonic matter, such as in neutron stars. So far, only indirect measurements anchored to the binding energies of nuclei can be used to constrain the three-nucleon force, and if hyperons are considered, the scarce data on hypernuclei impose only weak constraints on the three-body forces. In this work, we present the first direct measurement of the p-p-p and p-p-Lambda systems in terms of three-particle correlation functions carried out for pp collisions at root s = 13 TeV. Three-particle cumulants are extracted from the correlation functions by applying the Kubo formalism, where the three-particle interaction contribution to these correlations can be isolated after subtracting the known two-body interaction terms. A negative cumulant is found for the p-p-p system, hinting to the presence of a residual three-body effect while for p-p-Lambda the cumulant is consistent with zero. This measurement demonstrates the accessibility of three-baryon correlations at the LHC.

EUROPEAN PHYSICAL JOURNAL A 59[7], 145, 2023. DOI: 10.1140/epja/s10050-023-00998-6

[P225-2023] "Two-particle transverse momentum correlations in pp and p-Pb collisions at energies available at the CERN Large Hadron Collider"

Acharya, S.; Adamova, D.; **Chinellato, D. D.*; Guardiano, G. G.*; Jahnke, C.*; Takahashi, J.***; et al.
ALICE Collaboration

Two-particle transverse momentum differential correlators, recently measured in Pb-Pb collisions at energies available at the CERN Large Hadron Collider (LHC), provide an additional tool to gain insights into particle production mechanisms and infer transport properties, such as the ratio of shear viscosity to entropy density, of the medium created in Pb-Pb collisions. The longitudinal long-range correlations and the large azimuthal anisotropy measured at low transverse momenta in small collision systems, namely pp and p-Pb, at LHC energies resemble manifestations of collective behavior. This suggests that locally equilibrated matter may be produced in these small collision systems, similar to what is observed in Pb-Pb collisions. In this work, the same two -particle transverse momentum differential correlators are exploited in pp and p-Pb collisions at ./s = 7 TeV and ,./sNN = 5.02 TeV, respectively, to seek evidence for viscous effects. Specifically, the strength and shape of the correlators are studied as a function of the produced particle multiplicity to identify evidence for longitudinal broadening that might reveal the presence of viscous effects in these smaller systems. The measured correlators and their evolution from pp and p-Pb to Pb-Pb collisions are additionally compared to predictions from Monte Carlo event generators, and the potential presence of viscous effects is discussed.

PHYSICAL REVIEW C 107[5], 054617, 2023. DOI: 10.1103/PhysRevC.107.054617

[P226-2023] "Two-photon absorption in colloidal semiconductor nanocrystals: a review"

Alo, A.*; Lemus, J. C.*; Sousa, C. A.*; Nagamine, G.*; Padilha, L. A.*

Large two-photon absorption (2PA) cross-section combined with high emission quantum efficiency and size-tunable bandgap energy has put colloidal semiconductor nanocrystals (NCs) on the vanguard of nonlinear optical materials. After nearly two decades of intense studies on the nonlinear optical response in quantum-confined semiconductors, this is still a vibrant field, as novel nanomaterials are being developed and new applications are being proposed. In this review, we examine the progress of 2PA research in NCs, highlighting the impact of quantum confinement on the magnitude and spectral characteristics of this nonlinear response in semiconductor materials. We show that for NCs with three-dimensional quantum confinement, the so-called quantum dots, 2PA cross--section grows linearly with the nanoparticle volume, following a universal volume scaling. We overview strategies used to gain further control over the nonlinear optical response in these structures by shape and heterostructure engineering and some applications that might take advantage of the series of unique properties of these nanostructures.

JOURNAL OF PHYSICS-CONDENSED MATTER 35[49], 493001, 2023. DOI: 10.1088/1361-648X/acf4dc

[P227-2023] "Underlying-event properties in pp and p-Pb collisions at root(NN)-N-s=5.02 TeV"

Acharya, S.; Adamova, D.; **Chinellato, D. D.*; Guardiano, G. G.*; Jahnke, C.*; Takahashi, J.***; et al.
ALICE Collaboration

We report about the properties of the underlying event measured with ALICE at the LHC in pp and p-Pb collisions at root sNN = 5.02 TeV. The event activity, quantified by charged--particle number and summed- pT densities, is measured as a function of the leadingparticle transverse momentum (p(T) (trig)). These quantities are studied in three azimuthalangle regions relative to the leading particle in the event: toward, away, and transverse. Results are presented for three different p(T) thresholds (0.15, 0.5 and 1 GeV/c) at midpseudorapidity (|eta| < 0.8). The event activity in the transverse region, which is the most sensitive to the underlying event, exhibits similar behaviour in both pp and p-Pb collisions, namely, a steep increase with p(T)(trig) for low p(trig) (T), followed by a saturation at p(T)(trig) approximate to 5 GeV/c. The results from pp collisions are compared with existing measurements at other centre-ofmass energies. The quantities in the toward and away regions are also analyzed after the subtraction of the contribution measured in the transverse region. The remaining jet-like particle densities are consistent in pp and p-Pb collisions for p(trig) (T) > 10 GeV/c, whereas for lower p(T)(trig) values the event activity is slightly higher in p-Pb than in pp collisions. The measurements are compared with predictions from the PYTHIA 8 and EPOS LHC Monte Carlo event generators.

JOURNAL OF HIGH ENERGY PHYSICS [6], 23, 2023. DOI: 10.1007/JHEP06(2023)023

[P228-2023] "W-+/--boson production in p-Pb collisions at root sNN=8.16 TeV and Pb-Pb collisions at root sNN=5.02 TeV"

Acharya, S.; Adamova, D.; **Chinellato, D. D.*; Guardiano, G. G.*; Jahnke, C.*; Takahashi, J.***; et al.
ALICE Collaboration

The production of the W bosons measured in p-Pb collisions at a centre-of-mass energy per nucleon-nucleon collision root sNN = 8.16 TeV and Pb-Pb collisions at root sNN = 5.02 TeV with ALICE at the LHC is presented.

The W-+/- bosons are measured via their muonic decay channel, with the muon reconstructed in the pseudorapidity region -4 <eta(mu)(lab)< -2.5 with transverse momentum p(mu)(T)> 10 GeV/c. While in Pb-Pb collisions the measurements are performed in the forward (2.5 <y(cms)(mu)< 4) rapidity region, in p-Pb collisions, where the centre-of-mass frame is boosted with respect to the laboratory frame, the measurements are performed in the backward (-4.46 <y(cms)(mu)< -2.96) and forward (2.03 <y(cms)(mu)< 3.53) rapidity regions. The W- and W+ production cross sections, lepton-charge asymmetry, and nuclear modification factors are evaluated as a function of the muon rapidity. In order to study the production as a function of the p-Pb collision centrality, the production cross sections of the W- and W+ bosons are combined and normalised to the average number of binary nucleon-nucleon collision < N-coll >. In Pb-Pb collisions, the same measurements are presented as a function of the collision centrality. Study of the binary scaling of the W-+/--boson cross sections in p-Pb and Pb-Pb collisions is also reported. The results are compared with perturbative QCD calculations, with and without nuclear modifications of the Parton Distribution Functions (PDFs), as well as with available data at the LHC. Significant deviations from the theory expectations are found in the two collision systems, indicating that the measurements can provide additional constraints for the determination of nuclear PDFs and in particular of the light-quark distributions.

JOURNAL OF HIGH ENERGY PHYSICS [5], 036, 2023. DOI: 10.1007/JHEP05(2023)036

[P229-2023] "µeV electron spectromicroscopy using free--space light"

Auad, Y.; Dias, E. J. C.; Tence, M.; Blazit, J. D.; Li, X. Y.; **Zagonel, L. F.***; Stephan, O.; Tizei, L. H. G.; Abajo, F. J. G. de; Kociak, M.

The authors present & mu;eV electron spectromicroscopy, a technique that combines free-space light and electron beams to achieve unmatched spatial and spectral resolution. This approach enables detailed investigation of photonic structures, promising advancements in microscopy and quantum optics.
The synergy between free electrons and light has recently been leveraged to reach an impressive degree of simultaneous spatial and spectral resolution, enabling applications in microscopy and quantum optics. However, the required combination of electron optics and light injection into the spectrally narrow modes of arbitrary specimens remains a challenge. Here, we demonstrate microelectronvolt spectral resolution with a sub-nanometer probe of photonic modes with quality factors as high as 10(4). We rely on mode matching of a tightly focused laser beam to whispering gallery modes to achieve a 10(8)-fold increase in light-electron coupling efficiency. By adapting the shape and size of free-space optical beams to address specific physical questions, our approach allows us to interrogate any type of photonic structure with unprecedented spectral and spatial detail.

NATURE COMMUNICATIONS 14[1], 4442, 2023. DOI: 10.1038/s41467-023-39979-0

Eventos publicados

[P230-2023] "Epileptogenic zone classification with functional connectivity and graph measures"

Carlos, B. M.*; Campos, B. M.; Alvim, M. K. M.; Patino, M. G.; Cendes, F.; **Castellano, G.***
IEEE

Epilepsy is one of the most common neurological diseases, and it has a great variety of possible diagnosis that can involve different treatments. The characterization of epileptogenic zones (EZs) is of extreme importance for the evaluation of patients, specially for pharmacoresistant epilepsy patients that are candidates for surgery. Many works have been showing that epilepsy interferes with brain network organization, in particular during seizures or epileptic discharges, although there is also indication that there are significant alterations during interictal periods. With most studies using intracranial electroencephalography (EEG), there are few results about the alterations present in regular EEG examinations that could be used to indicate the general location of the EZ in advance. This prior indication could be beneficial for a better understanding of network changes across the whole scalp. The aim of this work was to extract relevant information from patients with different EZs, using functional connectivity and graph measures from normal background EEG signals. Patients with EZs in the temporal and frontal lobe were included in this study. Our results reinforce that centrality graph measures from many areas of the scalp are useful in the distinction between patients with different EZs. We also found that connectivity in the alpha band can be used for EZ classification and might be of interest in future studies.

2023 11TH INTERNATIONAL IEEE/EMBS CONFERENCE ON NEURAL ENGINEERING, NER, Série de livros: International IEEE EMBS Conference on Neural Engineering, 2023. DOI: 10.1109/NER52421.2023.10123728

Correções

[Co002-2023] "Measurement of prompt and nonprompt charmonium suppression in PbPb collisions at 5.02 TeV (vol 78, 509, 2018)"

Sirunyan, A. M.; Tumasyan, A.; **Chinellato, J. A.*; Tonelli Manganote, E. J.***; et al.
CMS Collaboration

EUROPEAN PHYSICAL JOURNAL C 83[2], 145, 2023. DOI: 10.1140/epjc/s10052-023-11272-w

Artigo destaque de capa

[DC-2023] "Elastocaloric Effect in Graphene Kirigami"

Ribeiro Junior, L. A. R.; Pereira Junior, M. L. L.; **Fonseca, A. F.***

Kirigami, a traditional Japanese art of paper cutting,has recentlybeen explored for its elastocaloric effect (ECE) in kirigami-basedmaterials (KMs), where an applied strain induces temperature changes.Importantly, the feasibility of a nanoscale graphene kirigami monolayerwas experimentally demonstrated. Here, we investigate the ECE in GKrepresenting the thinnest possible KM to better understand this phenomenon. Through molecular dynamics simulations, we analyze the temperaturechange and coefficient of performance (COP) of GK. Our findings revealthat while GKs lack the intricate temperature changes observed inmacroscopic KMs, they exhibit a substantial temperature change ofapproximately 9.32 K (23 times higher than that of macroscopic KMs,which is about 0.4 K) for heating and -3.50 K for cooling.Furthermore, they demonstrate reasonable COP values of approximately1.57 and 0.62, respectively. It is noteworthy that the one-atom-thick-graphene configuration prevents the occurrence of the complex temperaturedistribution observed in macroscopic KMs.

NANO LETTERS 18[23], 8801-8807, 2023. DOI: 10.1021/acs.nanolett.3c02260 **(Artigo destaque de capa)**

***Autores da comunidade IFGW**
Fonte: Web of Science on-line (WOS)

Defesas de Dissertações do IFGW

[D018-2023] "A Influência do Substrato ITO nas Propriedades Eletrônicas e Ópticas de Monocamadas de WSe2"
Aluno: Thiago Gonzalez-Llana Brito
Orientador: Prof. Dr. Luiz Fernando Zagonel
Data: 25/09/2023

[D019-2023] "Espectroscopia em terahertz de óxidos magnéticos"
Aluno: Giovanni Budroni Netto
Orientador: Prof. Dr. Flávio Caldas da Cruz
Data: 26/09/2023

[D020-2023] "Síntese e caracterização dos compostos intermetálicos RCuBi2 (R = Tb, Dy, Ho, Er)"
Aluno: Henrique Bazanella Pizzi
Orientador: Prof. Dr. Pascoal José Giglio Pagliuso
Data: 29/09/2023

[D021-2023] "Observação de supernovas e estimativa de distâncias usando detectores de neutrinos"
Aluno: Pedro Henrique Pinheiro Cintra
Orientador: Prof. Dr. Ernesto Kemp
Data: 04/10/2023

[D022-2023] "Caracterização de dicalcogenetos de metais de transição usando micro-reflectância geração e geração do sinal de segundo harmônico"
Aluno: Daniel Schmitz Bertini
Orientador: Prof. Dr. Odilon Divino Damasceno Couto Junior
Data: 31/10/2023

Defesas de Teses do IFGW

[T011-2023] "Efeitos de Descoerência Quântica em Neutrinos de Supernovas"
Aluno: Marcos Vinicius dos Santos
Orientador: Prof. Dr. Pedro Cunha de Holanda
Data: 05/10/2023

[T012-2023] "Decaimentos de Mésons Carregados em Modelos com Conservação Natural de Sabor"
Aluno: Sany Willian Ponce Novelo
Orientador: Prof. Dr. Marcelo Moraes Guzzo
Data: 06/10/2023

Fonte: Portal IFGW/Eventos
Disponível em: https://portal.ifi.unicamp.br/a-instituicao/eventos/month.calendar/2023/10/27/-

Defesas de Dissertações e Teses do PECIM

Observação: Não ocorreram neste período defesas de teses e dissertações, com orientadores ou banca do IFGW, do Programa de Pós-Graduação Multiunidades em Ensino de Ciências e Matemática – Mestrado e Doutorado (PECIM) da Unicamp.

Fonte: Página do PECIM
Disponível em: https://www.pecim.unicamp.br/bancas

Abstracta

Instituto de Física
Diretor: Profa. Dra. Mônica Alonso Cotta
Diretora Associada: Prof. Dr. Marcos Cesar de Oliveira
Universidade Estadual de Campinas - UNICAMP
Cidade Universitária Zeferino Vaz
13083-859 - Campinas - SP - Brasil
e-mail: secdir@ifi.unicamp.br
Fone: +55 19 3521-5300

Publicação

Biblioteca do Instituto de Física Gleb Wataghin
http://portal.ifi.unicamp.br/biblioteca
Instagram: @bif.unicamp

Diretora Técnica: Sandra Maria Carlos Cartaxo
Coordenadora da Comissão de Biblioteca: Profa. Dra. Arlene Cristina Aguilar

Elaboração:
Maria Graciele Trevisan (Bibliotecária)
contato: infobif@ifi.unicamp.br